CHARLES UNIVERSITY

Faculty of Science

Department of Biochemistry

Study programme: Biochemistry

Teodor Traub

Notch interaction with glycogen synthase kinase 3b in neurodegenerative disease

Interakce glykogensyntázakinázy-3β v neurodegenerativních onemocněních

Supervisor: Mgr. Jan Mašek, PhD

Consultant: RNDr. Petr Novák, PhD

Prague 2024

Prohlášení:

Prohlašuji, že jsem závěrečnou práci zpracoval/a samostatně a že jsem uvedl/a všechny použité informační zdroje a literaturu. Tato práce ani její podstatná část nebyla předložena k získání jiného nebo stejného akademického titulu.

[I affirm this thesis was elaborated independently, that all sources used were cited properly and that any part of the thesis has not been submitted for obtaining another degree.]

V Praze, 24. 5. 2024 _____

Acknowledgements

I would like to thank my cat. And also,

I would like to express my sincere gratitude to my supervisor, Mgr. Jan Mašek, PhD for all his guidance and encouragement. I thank Hana and Fabio for their patience and assistance throughout my work in the lab, and Anna, Daniel and František for being always ready to help. I would like to thank my consultant RNDr. Petr Novák, PhD for providing proteomic data and helping to bring my project into being.

Abstract

Glycogen synthase kinase-3βeta (GSK-3β) is a serine/threonine protein kinase involved in a number of signaling processes. Pharmacological inhibition of GSK-3β has been shown to have neuroprotective effects, and its dysregulation is present in a variety of neurodegenerative, neuromuscular, developmental, and psychiatric disorders. GSK-3β is an essential component of the canonical Wnt pathway, which is involved in nervous system development. Notch signaling, like Wnt, plays a key role in development, but its relationship to GSK-3β remains unclear. The existing literature indicates that GSK-3 phosphorylates Notch intracellular domain but contradicts whether GSK3β affects Notch positively or negatively. Thus, such molecular "cross-talk" is highly complex and interactions may exist at multiple levels beyond simple phosphorylation with other components being involved. Myotonic dystrophy is a genetic neuromuscular disease that causes dysregulated protein expression of many proteins, including GSK-3β, and features developmental, muscle, and neurological symptoms. Studying molecular interactions in the context of myotonic dystrophy may help uncover effects that GSK-3β and Notch have on development and disease of nervous and muscular systems.

This thesis presents a review of previous studies concerning the relationship between GSK-3 and Notch and reports my attempts to expand on past research using a different approach. VDAC1, a protein reportedly interacting with both GSK-3β and N1ICD was selected from GSK-3β interactome in myotonic dystrophy muscle cells (unpublished mass spectrometry results provided Laboratory of Structural Biology and Cell Signaling) and the molecular “toolset” for further studies was prepared. GSK-3β, N1ICD and VDAC1 were visualized experimentally using immunocytochemistry and *in silico* using modern Alphafold-based techniques.

Keywords: GSK-3, Glycogen synthase kinase 3, Notch signaling, crosstalk, neurodegeneration, myotonic dystrophy, signal transduction, protein-protein interaction

Abstrakt

Glykogensyntázakináza-3β (GSK-3β) je serin/threoninová proteinkinása účastnící se řady signálních procesů. Farmakologická inhibice GSK-3β má neuroprotektivní a neuroregenerativní účinky a a její dysregulace se vyskytuje u řady neurodegenerativních, neuromuskulárních, vývojových a psychiatrických poruch. GSKB3 je základní součástí kanonické dráhy Wnt, která se podílí na vývoji nervové soustavy. Signalizace Notch, stejně jako Wnt, hraje klíčovou roli ve vývoji, ale její vztah ke GSK-3β zůstává nejasný. Existující literatura uvádí, že GSK-3 fosforyluje intracelulární doménu Notch, ale rozchází se v tom, zda GSK3β ovlivňuje signalizaci Notch pozitivně nebo negativně. Takový molekulární "cross-talk" je velmi komplexní a kromě prosté fosforylace mohou interakce existovat na více úrovních za účasti dalších proteinů. Myotonická dystrofie je genetické nervosvalové onemocnění, které způsobuje dysregulovanou expresi mnoha proteinů, včetně GSK-3β, a vyznačuje se vývojovými, svalovými a neurologickými příznaky. Studium molekulárních interakcí v kontextu myotonické dystrofie může pomoci odhalit účinky, které mají GSK-3β a Notch na vývoj a onemocnění nervové a svalové soustavy.

Tato práce představuje přehled předchozích studií týkajících se vztahu mezi GSK-3 a Notch a uvádí mé pokusy o rozšíření předchozího výzkumu s použitím jiného přístupu. Z interaktomu GSK-3β ve svalových buňkách myotonické dystrofie byl vybrán protein VDAC1, který údajně interaguje jak s GSK-3β, tak s N1ICD (nepublikované výsledky hmotnostní spektrometrie poskytla Laboratoř strukturní biologie a buněčné signalizace), a byly připraveny molekulární nástroje umožňující rozsáhlejší studium tématu. GSK-3β, N1ICD a VDAC1 byly vizualizovány experimentálně pomocí imunocytochemie a *in silico* pomocí moderních technik založených na Alphafold.

Klíčová slova: GSK-3, glykogen syntáza kináza 3, Notch signalizace, crosstalk, neurodegenerace, myotonická dystrofie, přenos signálu, proteinová interakce

Table of contents

List of Abbreviations

(Co) IP	(Co-)immunoprecipitation
ALS	Amytrophic lateral sclerosis
AMPK	AMP-activated protein kinase
APS	Ammonium peroxosulphate
BCA	Bicinchoninic acid
BSA	Bovine serum albumin
cDNA	Complementary deoxyribonucleic acid
CK	Casein kinase
DM (1, 2)	Myotonic dystrophy 1/2
ER, SR	Endoplasmic reticulum, sarcoplasmic reticulum
FBS	Fetal bovine serum
FGF	Fibroblast growth factor
GFP	Green fluorescent protein
GSK-3	Glycogen synthase kinase 3
HA tag	Hemagglutinin tag
HEK	Human embryonic kidney
HK2	Hexokinase 2
HRP	Horseradish peroxidase
IgG	Immunoglobulin G
LB	Lysogeny broth
MEF	Mouse embryonic fibroblast
MS	Mass spectrometry
mTOR	Mammalian target of rapamycin
MW	Molecular weight
NICD	Notch intracellular domain
PBS(T)	Phosphate buffered saline (with added Tween)
PCR	Polymerase chain reaction
PEI	Polyethyleneimine
Pen/strep	Mixture of penicillin and streptomycin
PLA	Proximity ligation assay
PTM	Post-translational modification
PVDF	Polyvinylidene fluoride
SDS PAGE	Sodium dodecyl sulfate–polyacrylamide gel electrophoresis
TAE	Tris-acetate + ethylenediaminetetraacetic acid
TBS(T)	Tris buffered saline (with added Triton 100)

TEMED	Tetramethylethylenediamine
VDAC1	Voltage-dependent anion channel
WB	Western blot

Non-SI units

bp	Base pairs, used for double stranded DNA length
g	Gravity, used for relative centrifugal force
Da	Dalton, used for molecular mass (or molecular weight, MW), identical value to atomic mass constant
RPM	Rotation per minute
°C	Degree celsius, equivalent to value in Kelvin + 273.15
% (w/v), (w/w), (v/v); x:x	Percentage, used for concentration of solutions. Calculated either as ratio of mass of solute to total volume (w/v; with 1 kg equivalent to 1 dm^3), mass of solute to total mass (w/w) or volume of solute to total volume (v/v). Concentrations of antibodies are given as dilution ratio of volume of stock to volume of solvent, as per convention.

Abbreviations used as names for commercial products are not included in this section.

Part 1: Literature review

1.1 Glycogen synthase kinase-3

1.1.1 Introduction

"Phosphorylase a produced from phosphorylase b in the presence of ^{32}P-ATP has been isolated and found to contain firmly bound isotopic phosphate," [1] that is how biochemists Edmond Fischer and Edwin Krebs summarize the findings of their 1956 study, almost forty years later awarded with a Nobel Prize [2]. They identified the first kinase, an enzyme catalyzing the transfer of a phosphate group from ATP to another substrate. What became evident in the following years was that this enzyme was not unique – the human "kinome" alone counts more than 500 kinases [3] and they can be considered highly conserved and at the same time very diverse [4]. Why that is not necessarily a contradiction is well demonstrated by glycogen synthase kinase 3 (GSK-3), at its core resembling a textbook kinase example with no additional functional domains but uses the few tools available in less usual ways.

The most apparent GSK-3's feature is constitutive activity – it is active in steady state, phosphorylating its substrates, while upstream signaling effectors, usually in the form of other protein kinases, inhibit its kinase activity [5]. The inverse activity of GSK-3 is crucial for the glycogen metabolism, as the cell's glycogen synthesis is inhibited by phosphorylation of glycogen synthase until it receives a signal, for example through the insulin receptor, GSK-3 stops phosphorylating glycogen synthase, triggering glycogen synthesis [6]. This function gave it its name, after it was initially isolated from rabbit muscle [7] (it also gave names to GSK-1 [8], GSK-2 [9] GSK-4 and GSK-5 [10]; none of these are in use).

Soon after the discovery of GSK-3's function in glycogen metabolism and insulin signaling, further studies revealed multiple other roles of GSK-3 in the cell[1]. The enzyme attracted attention after being demonstrated to phosphorylate substrates such as the transcription factor and oncogene c-Jun or tau protein, characteristic for Alzheimer's disease [11], [12]. In 1992, Siegfried and colleagues described the mechanism of Drosophila *wingless* signaling including the repression by the insect homologue of GSK-3 [13]. In mammals, wingless

[1] This can be seen by using the NCBI search service Pubmed search for all articles mentioning "glycogen synthase" – around results 22 000 as of 1/2024, and compare that to all articles mentioning "glycogen synthase" but not including "kinase-3" – only around 7 500 results as of 1/2024 [149]

signaling is known as Wnt and wingless/Wnt is one of the major developmental signaling pathways in all animals [14].

1.1.2 Structure and catalytic activity

In mammals, two paralogs of GSK-3 were found: GSK-3α and the more studied GSK-3β [15]. GSK-3α and GSK-3β consist of 483 and 420 amino acids respectively, and one rarer alternatively spliced isoform of GSK-3β, consisting of 433 amino acids, has been described as well [16], [17]. The eukaryotic kinases are broadly divided into three groups: serine/threonine-protein kinases, tyrosine-protein kinases, and dual-specificity protein kinases. GSK-3 is a serine/threonine-protein kinase. The subfamily of GSK-3 includes the well characterized GSK-3α and GSK-3β of vertebrates or Shaggy kinase of drosophila, but also a large number of GSK-3-like kinases in non-animal eukaryotes, such as various plants [18].

The first crystallographic studies of GSK-3β dating revealed phosphorylation sites involved in the mechanisms regulating GSK-3β activity [19], [20]. Today, PDB lists 99 different structures of GSK-3β and its complexes, all solved by X-ray crystallography [21].

GSK-3's structure is defined by the catalytic domain, while the additional N- and C-terminal "domains" are disordered. Catalytic domain resembles that of many other kinases and includes the highly conserved glycine-rich sequence (although that is mostly absent in GSK-3β, reviewed in [22]), and catalytic aspartate, necessary for directing the substrate hydroxyl, and a single "signature" residue of all kinases [23]. This aspartate is preceded by arginine and that puts GSK-3 to the category of "RD" kinases, represented by majority [24].

GSK-3 has a wide range of various substrates and recognizes most of them by their already phosphorylated ("primed") serine/threonine. This is possible thanks to a positively charged binding pocket formed by several arginines/lysines, including the "RD" arginine [25], [26]. In GSK-3β these are Arg-96, Arg-180 (RD) and Lys205, as pictured in **Fig. 2** (page 12). GSK-3's catalytic core and primed phosphate-binding pocket (hereinafter referred to as binding pocket) are relatively close and the target Ser/Thr is usually located three amino acids from the primed residue in N-terminal direction (S/T-X-X-X-pS/pT motif) [27]. Already phosphorylated proteins make up most of known GSK-3 substrates – though there are some notable exceptions [28].

1.1.3 Regulation

The primed substrate recognition pocket serves another purpose – it is the basis of the best characterized mechanism of GSK-3 inhibition. That is inhibition by phosphorylation of its

N-terminal serine, Ser-9 in GSK-3β or Ser-21 in GSK-3α [29]. This serine is separated from the catalytic domain by a short but flexible disordered sequence and after being phosphorylated, it acts as a competitive inhibitor of primed substrate binding by displacing the substrates from the recognition pocket [30]. This could be reversed by increasing the concentration of substrates, true to the kinetics of competitive inhibition. The "constitutively active" S9A mutant of GSK-3β has an established use as a control in experiments [31], [32].

The list of kinases known to inactivate GSK-3 includes protein kinase A, protein kinase C and, perhaps most notably, protein kinase B (Akt) [33]. Akt is a component of phosphoinositide 3-kinase (PI3K) signaling pathway (reviewed in [34]), the cell's response to various stimuli, such as growth factors, anti-apoptotic signals, and importantly insulin. Insulin receptor activates PI3K which, through a cascade of different events, activates Akt. Akt acts as the central node in insulin signaling (**Fig. 1**), as it phosphorylates a large number of substrates which mediate different metabolic responses - besides GSK-3 phosphorylation, which initiates glycogen synthesis, there is activation of mammalian target of rapamycin (mTOR) – promoter of protein synthesis, marking of glucose transporters for their export to the cell membrane, or downregulation of transcription factor FoxO.

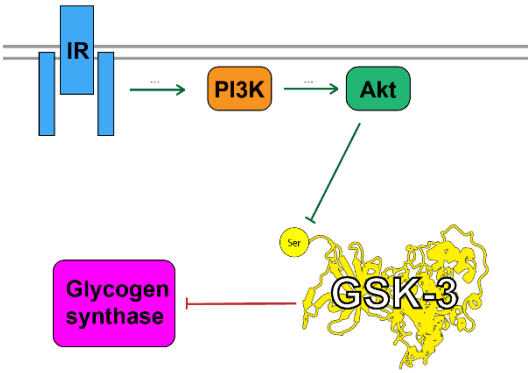

Fig. 1: Very simplified scheme of GSK-3's role in insulin signaling. In the off state, GSK-3 inhibits glycogen synthase by phosphorylation. After activation of insulin receptor (IR), PI3K becomes active and subsequently causes activation of Akt. Akt inhibits GSK-3, phosphorylating its N-terminal serine.

Phosphorylation on a tyrosine residue of GSK-3's activation loop has opposite effects, promoting its catalysis, although it appears to be present most of the time and believed to be a result of rapid autophosphorylation [35].

There are other ways of regulating the activity of GSK-3, such as previously mentioned priming, inter-substrate competition, formation protein complexes that mediate its contact with a specific substrate or intracellular vesicles. All of these can be demonstrated on a single signaling pathway – Wnt/β-catenin.

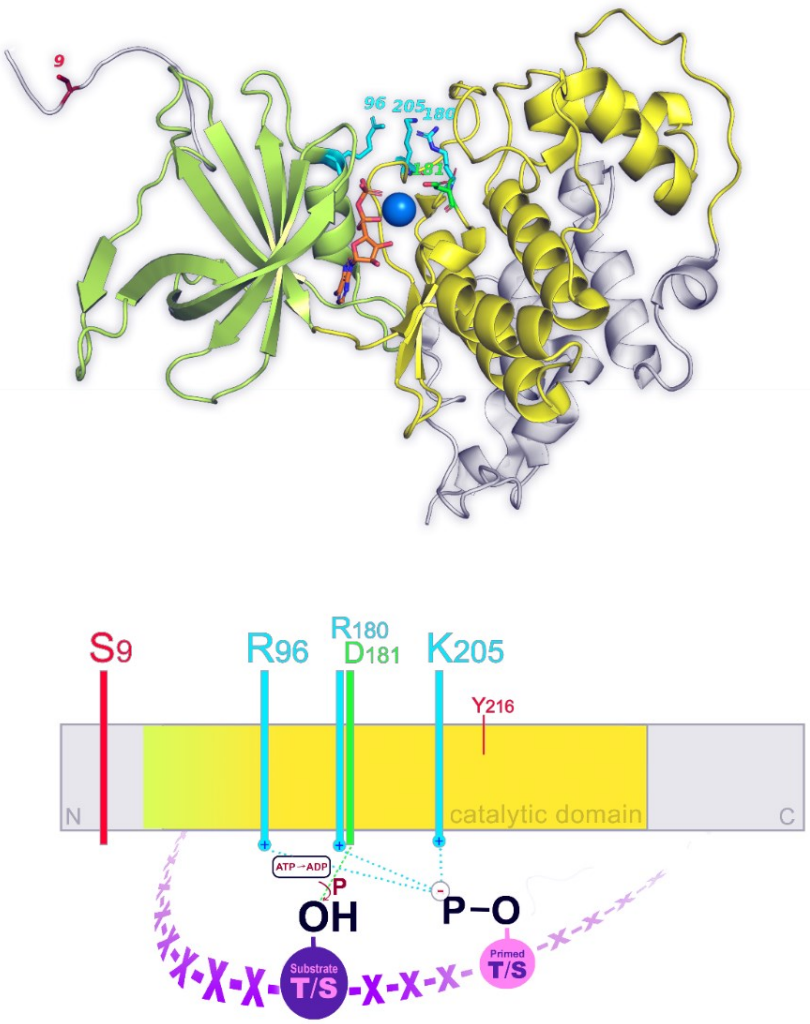

Fig. 2: The GSK-3β protein structure. (Top) GSK-3β structure [36] with important residues highlighted. Green and yellow mark the N-terminal and C-terminal lobes of the structurally conserved kinase catalytic domain. The gray N-terminal sequence is not modeled in the original PDB due to its disordered nature and was added manually to illustrate the position of Ser9. Catalytic center includes magnesium ion (blue) and ADP (orage), along with the essential catalytic aspartate (green) and basic residues for primed substrate recognition (cyan). (Bottom) Scheme of GSK-3β protein based on, additionally showing Tyr216. The primed substrate sequence is represented in purple. "P" symbolizes phosphate, not phosphorus.

1.2 Glycogen synthase kinase-3 in Wnt/β-catenin signaling

1.2.1 Introduction

The unusual word Wnt, denoting a large family secreted ligand proteins [37] and the three completely distinct cascades they activate (reviewed in [38]), came into being after it was discovered [39] that mammalian cancer-related proteins "int" are in fact highly conserved homologues of the Drosophila protein family "wingless" [39]. In most cases [40], however, "Wnt" is intended to be synonymous with Wnt/β-catenin pathway, also known as the canonical Wnt pathway.

Wnt/β-catenin signaling is essential both for embryonic development, adult homeostasis, and when deregulated, often leads to cancer [41]. The pathway is activated through a Frizzled receptor, which is homologous to G-protein coupled receptors (GPCRs) albeit mechanistically completely different from most of them [42]. Upon activation by a Wnt protein, signal is further transferred through interaction with the cytoplasmic phosphoprotein Disheveled. The membrane-bound Disheveled can subsequently disrupt the function of β-catenin destruction complex (DC). Biochemical characterization of this large assemblance of proteins has been a long challenging task with the initial lead, and a starting point for many early contributions, being the presence of GSK-3 [13], [43], [44], [45], [46]. DC inherits GSK-3's inverse activity and Disheveled-mediated inhibition of GSK-3 terminates the constitutive phosphorylation-dependent degradation of β-catenin, allowing it to translocate to the nucleus and alter gene expression.

1.2.2 Beta-catenin destruction complex

The primary structure of β-catenin makes it a standard GSK-3 substrate. Its Ser-45 is phosphorylated by casein kinase 1 (CK1), the priming kinase, which allows GSK-3 to sequentially phosphorylate Thr-41, Ser-37 and Ser-33 [45]. However, even though the priming site is followed by three perfect GSK-3 consensus motifs, priming by CK1 is not enough for the phosphorylation process to begin. Other DC components, Axin and Adenomatous polyposis coli (APC) act as scaffolds and bind β-catenin. Ranes et al. provided a good demonstration of structural and enzymatic functions of individual DC components by reconstituting the complex from purified proteins, in some experiments also with purified ubiquitination enzymatic apparatus and 26S proteasome [47]. It shows evidence of how APC and Axin influence phosphorylation and highlight the central role of GSK-3β in the whole process.

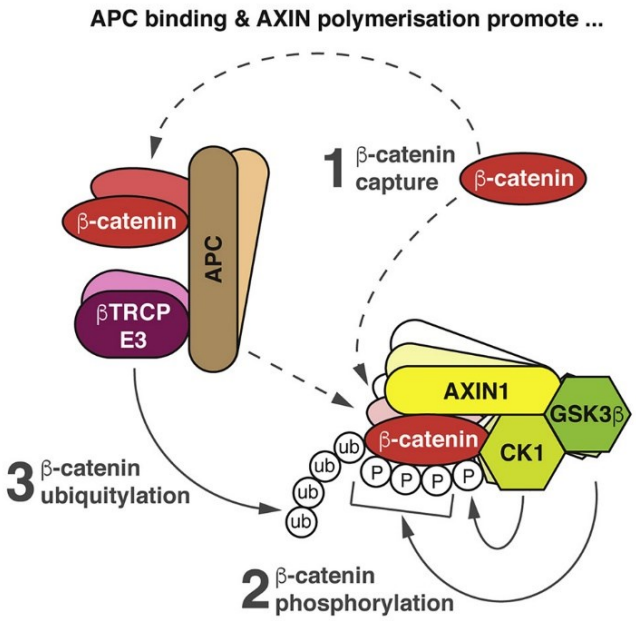

Fig. 3: Destruction Complex scheme. APC is necessary for the phosphorylation of beta catenin – allows for its capture (1) and directs it to the Axin-kinases complex (2). The subsequent ubiquitination was also shown to require APC, as it is likely involved in the recruitment of E3 enzyme (3). Axin, which captures APC-bound beta catenin, is usually present as a polymer of variable length; the degree of polymerization was found to affect kinase activity of DC. Illustration created by the study's authors, reproduced and unmodified from [47].

1.2.3 Inhibition of GSK-3

Intriguingly, GSK-3β inhibition by Wnt is independent of the well characterized Ser9 phosphorylation [48]. After this discovery, extensive research of biochemical mechanisms involved in Wnt pathway followed and multiple distinct models of Wnt-mediated GSK-3β inhibition were proposed [49]. After Wnt activation, GSK-3β can target the phosphoserine of frizzled-interacting transmembrane protein low-density lipoprotein receptor-related protein 6 (LRP6) which, being more kinetically favorable than phosphorylation of β-catenin, acts as a competitive inhibitor. Additionally, it has been observed that the membrane-bound protein complexes undergo endocytosis by multivesicular bodies, this could also prevent GSK-3β from targeting β-catenin [50] . Recent publications have both challenged [51] and supported [52] the relevance of endocytosis/membrane trafficking in Wnt signaling.

In addition to the canonical role in Wnt/β-catenin signaling, GSK-3 appears to regulate signal transduction by interaction with the components of other biochemical pathways.

However, the signaling function of GSK-3 outside Wnt/β-catenin and PI3K/Akt is not well characterized, and the proposed biochemical mechanisms are often conflicting. An intriguing example is the GSK-3 crosstalk with Notch signaling.

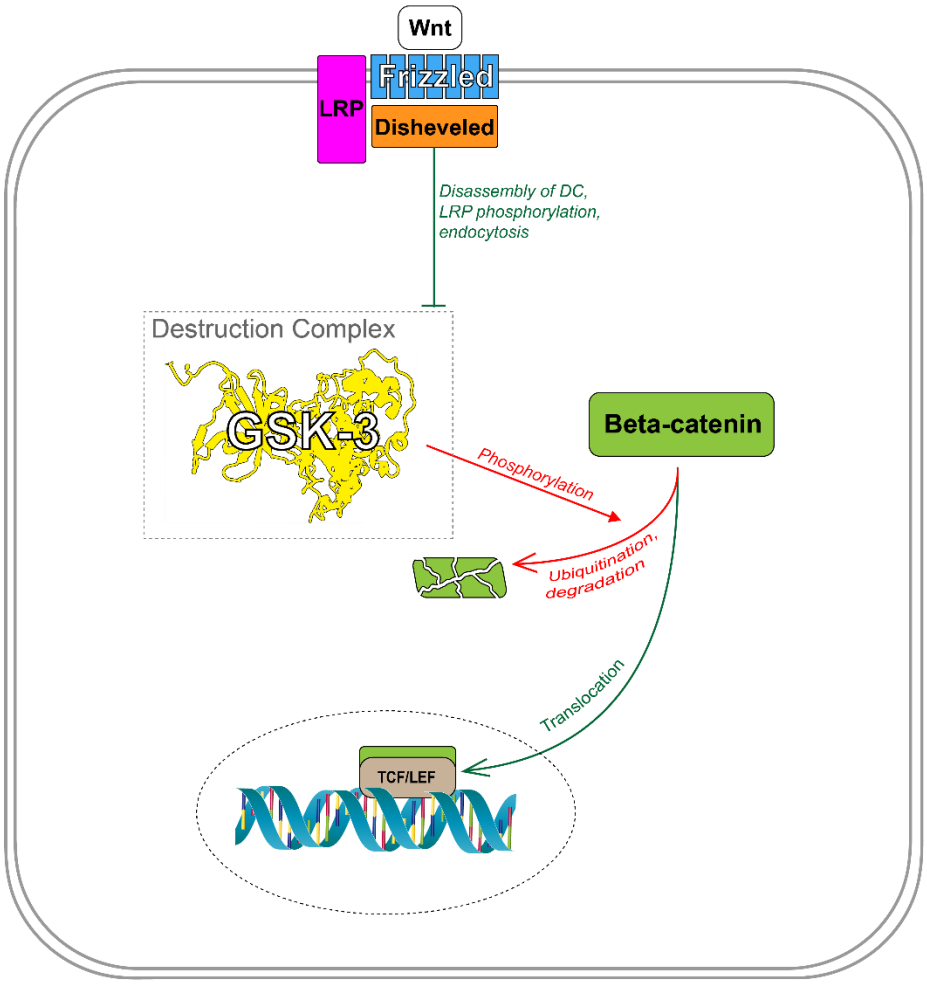

Fig. 4: Simple overview of Wnt/β-catenin pathway. Without stimulation, GSK-3 phosphorylates β-catenin, causing its degradation. After Wnt binds Frizzled, GSK-3 becomes inhibited and β-catenin can accumulate in the nucleus and alter transcription.

1.3 Glycogen synthase kinase-3 and Notch signaling

1.3.1 Canonical Notch pathway

The first observations of Notch signaling come from as early as 1914 when John S. Dexter noticed notched the notched appearance of the wings of some Drosophila melanogaster specimens [53]. Thomas H. Morgan, American biologist who first recognized the usefulness of Drosophila melanogaster as a model for genetic research, then characterized the gene responsible for the notched wing phenotype as a X chromosome-linked gene whose biallelic mutation is lethal [54], [55]. Nowadays it is known that Notch signaling is one of the integral molecular mechanisms that animal cells use to communicate with each other in order to form complex multicellular systems [56]. As such, it is highly evolutionary conserved, and present in all metazoan animals, with homologues existing also within the genomes of plants, bacteria or protists [57].

What makes its emerging molecular interactions with additional biochemical systems specially interesting is its "simple" architecture. The architecture of most signaling pathways is composed of a cascade of distinct proteins that pass the "signal" one to another, commonly utilizing de/phosphorylation, conformation change, alteration of enzymatic activity or recruitment of non-macromolecular mediators – "secondary messengers". However, Notch signaling pathway doesn't have such cascade and, in essence, the signal is carried by a sole protein – Notch receptor [55]. In this aspect, Notch signaling has more in common with signaling by nuclear receptors (reviewed in [58]) but unlike them, Notch receptors are transmembrane proteins and directly in contact with extracellular environment.

Signal transduction through the "canonical" Notch pathway begins when a ligand binds to the Notch receptor extracellular domain (NECD). Uniquely, these ligands are also membrane proteins partially homologous to Notch receptors, which means that the activation of Notch requires direct contact of two cells – referred to as signal sending and signal receiving cell. This makes Notch signaling a form of asymmetrical cell-cell interaction [59], and allows for the emergence of unique mechanisms involved in the complex patterning needed for animal development [60], [61]. It has been shown that the mechanical "pulling" force, generated by endocytosis of the ligand, induces a conformational change of Notch receptor and the two subsequent proteolytic cleavages. A protease known as ADAM (a disintegrin and metalloprotease) targets and cleaves Notch receptor at a newly exposed site; this is known as site 2 (S2) cleavage [62], [63]. The following S3 cleavage, catalyzed by γ-secretase, releases the intracellular domain of Notch (NICD) into the cytosol (reviewed in [64]). Cleaved NICD

localizes to the nucleus where it forms transcriptional complex, with DNA-binding protein CSL (acronym for the orthologues CBF1/RBP-jk - mammals, Su(H) - Drosophila, Lag-1 - Caenorhabditis elegans) [65] and a protein of the mastermind family (in mammals called MAML – mastermind-like) [66], and drive expression of the Notch target genes.

1.3.2 Regulation of Notch receptor activity

Notch receptors are large transmembrane proteins (all four human isoforms contain at least 2000 amino acids) and are formed by the extracellular (NECD), intracellular (NICD) and transmembrane (TM) domain. Fully functional Notch receptor has quaternary structure, as its processing in Golgi apparatus includes proteolysis into two chains linked by non-covalent interactions [67] - S1 cleavage. Other characteristic post-translational modification of NECD is O-glycosylation, (most notably the additions of fucose or N-acetylglucoasamine), which is a major way of regulating receptor-ligand contacts [63]. Although the research of receptor-ligand binding and "Notch glycobiology" is itself an expansive and active field (reviewed in [68]), this thesis is about processes happening inside the cells and thus concerns the NICD.

Because no amplification step is present (in other pathways the output signal intensity is often amplified by several orders of magnitude – for example, this ratio in MAPK pathway measured around 10^6 as calculated by Chen and Wu [69]), while even subtle alteration of Notch protein activity or levels, such as changes in expression, post-translational modifications (PTMs), or protein-protein interactions (PPIs), can alter the outcome of the signaling, and lead to disease (reviewed in [70]).

In canonical Notch signaling, NICD is essentially a transcriptional co-factor, but growing number of studies show evidence of its interactions with other biochemical systems and how it mutually modulates other signaling pathways [71]. Developmental biologists have been aware of a link between the pathways of Notch and Wnt (or wingless in Drosophila) for more than 20 years [72], but the molecular mechanisms behind it are not well understood. This is especially true for the relationship between Notch and Wnt's key component GSK-3, where results of both *in vitro* and *in vivo* experiments have been inconsistent and often conflicting (**Table 1**).

1.3.3 Notch and GSK-3

The involvement of GSK-3β in Notch signaling was first proposed in a study of homologous proteins in Drosophila neural development [73]. A 2002 research article by Foltz et al showed evidence of GSK-3β phosphorylating the intracellular domain of Notch1 in mammalian cells,

[73] positively regulating Notch signaling, possibly by protection of N1ICD from degradation in proteasome [74]. Expression of Hes1, the major Notch1-regulated gene, was decreased in GSK-3β null mouse embryonic fibroblasts (MEFs) compared to control, wild type MEFs. Mouse N2a neuroblastoma cells treated with LiCl (an GSK-3β inhibitor, with relatively low target specificity [75]) showed decrease in N1ICD concentration in the span of 4 hours. To support the hypothesis of GSK-3 protecting NICDs from degradation, they reported that in proteasome inhibitor-treated samples, GSK-3β manipulation affected Notch signaling to a lesser degree.

In the following years, a study by Espinosa and colleagues reported that GSK-3β regulated Notch2 signaling negatively, as observed in HEK-293T cells [76]. Another study showed negative regulation of Notch1 signaling, this time in MEF cells, a conclusion which contradicts with Foltz and colleagues [77]. This study also suggested that the phosphorylated residues on Notch1 were Thr1851, 2123, and 2125. However, this was performed using truncated N1ICD constructs and comparing their change in intensity after LiCl treatment.

An in vivo study by Kim et al focused on the role of GSK-3 in neural progenitor homeostasis, a process in which Notch signaling is essential [78]. They produced Gsk3α-null mice, as well as loxP-flanked Gsk3β, excised by Cre recombinase expressed in Nestin-positive cells - resulting in conditional deletion of Gsk3β in neural progenitors. As apparent from immunohistochemistry and western blots of 14-day embryonic (E14) telencephalon, the $Gsk3\alpha^{-/-}$; $Gsk3\beta^{loxP/loxP}$ brains showed higher distribution of undifferentiated progenitors, which correlated with the upregulation of Notch target genes Hes1 and Hes5. NICD itself was also upregulated. It is not clear to what extent this is the observed phenotype caused by upregulated β-catenin signaling and to which by altered NICD activity. However, inhibition of β-catenin effects by dominant-negative form of Wnt effector transcription factor TCF only partially suppressed the maintenance of progenitors in culture, suggesting a Wnt-independent effect of GSK-3 on Notch-mediated cellular response. The article shows that GSK-3 is important negative regulator of several signaling pathways in embryonic brain development but stopped short of dissection of the underlying molecular mechanisms [78].

Zheng and Conner produced results consistent with negative regulation. Knocking down GSK-3β with siRNA in U2OS cells resulted in a significant increase in measured Notch signaling activity, and so did inhibition with a specific inhibitor [79]. A time dependent increase in Notch receptors on membrane was observed, at least partly related to the enhanced endosomal recycling, as supported by immunofluorescence experiments.

Conversely - in vascular smooth muscle cells, GSK-3β was shown to positively regulate Notch signaling and proliferation [80]. Activity of both GSK-3 and Notch was observed to correlate with MAPK/ERK signaling, suggesting it as their main upstream regulator.

Notch signaling is also widely studied in the context of leukemia. De Falco et al suggests that in chronic lymphoblastic leukemia GSK-3β affects Notch signaling negatively, and, at least partially, by assisting with the degradation of NICD. This was supported by proximity assays of GSK-3β – Notch – ubiquitin and modulating GSK-3β by specific inhibitors and known upstream regulators – Akt, PP2A [81].

Additional phosphorylation sites were suggested to be in N1ICD's nuclear localization signal (NLS) by Han et al. Their results indicate that these residues (Thr2122, Thr2124, Ser2126, Thr2128) need to be phosphorylated in order to initiate transport of N1ICD to the nucleus [82].

Table 1: Overview of major publications focused on GSK-3/Notch cross-talk. Colored based on whether the authors identified GSK-3 as a positive (green) or negative (red) regulator of Notch signaling. IP – immunoprecipitation, WB – western blot, IF – immunofluorescence, PLA – proximity ligation assay.

Study	Cells	Manipulation with GSK-3	Detection of Notch	Detection of Notch phosphorylation	Notch isoform	GSK-3 isoform	Conclusions
Foltz et al, 2002 [55]	MEF, N2a	LiCl, dominant-negative mutant	Hes1-luciferase assay, pulse-chase analysis, IP/WB	in vitro assay based on treatment with GSK-3 in presence of ^{32}P-labeled ATP	1	β	GSK-3β phosphorylates N1ICD and protects it from degradation, positively regulating Notch
Espinosa et al, 2003 [57]	HEK-293T, NIH-3T3 (mef),	LiCl, Wnt1	IP/WB, IF, Hes1-luciferase assay	^{32}P labeling, site identification using different NICD fragments	2 (ICD and full-length)	β	GSK-3β phosphorylates T2068, S2070, T2074, T2093 of N2ICD, but not full length N2, inhibits target transcription. Notch affects localization of GSK-3β
Kim et al, 2009 [59]	Mice (13 – 17E)	Cre + loxP of Gsk3β , KO of Gsk3α	Histological analyses, IF (Hes1), WB, comparison with other developmental pathways	Indirect	1, but mostly indirect – (Hes1, phenotype)	α, β	GSK-3 inhibits NICD and Hes1 in vivo, inhibits neural stem cell maintenance, partially Notch-dependent unrelated to Wnt
Jin et al, 2009 [58]	MEF	LiCl, siRNA	IP/WB, RT-PCR, luciferase assay	Site identification using truncated N1ICD	1 (full-length, ICD, fragments)	α , β	GSK-3β decreases expression of N1ICD, Hes1, phosphorylates at T1851, 2123, and 2125. GSK-3α, interacts with Notch1.
Guha et al, 2011 [61]	Rat vascular SMC	SB-216763, siRNA, transfection with S9A mutant	IF, WB, RT-PCR of target genes Hrt1 and Hrt3. proliferation and viability assays	Indirect	1, 3	β	GSK-3β positively regulates levels of N1ICD1 N3ICD, Hrt-3, promoting vSMC proliferation
Han et al, 2012 [63]	HEK293T, Cos7	Transfection with WT and dominant negative, LiCl	Fluorescence of GFP-tag with focus on nuclear localization, IP/WB, luciferase assay	32P labeling, site identification using truncated N1ICD	1 (ICD, derived fragments)	β	GSK-3β phosphorylates T2122, T2124, S2126, T2128 of N1ICD's NLS, promotes its transport to nucleus. These sites differ from the usual GSK-3β consensus
Zheng and Conner, 2017 [60]	HeLa, U2OS	siRNA, XXVII (specific inhibitor)	Luciferase assay, IF+ endosome localization, pulse chase analysis, WB	Indirect	1	β	GSK-3β negatively regulates Notch transport and recycling
De Falco et al, 2022 [62]	CLL patient-derived leukocytes	SB-216763, Akt inhibitor SB216763, PP2A activator DT-061	IP/WB, RT-PCR (Notch1, Hes1, Deltex), IF, PLA, IP, and PLA of Notch1-ubiquitin	Indirect	1-	β	GSK-3β inhibits Notch activity in CLL cells, promotes degradation. Akt and PP2A can serve as pharmacological targets for GSK-3β activation

1.4 Glycogen synthase kinase-3, Notch and muscular dystrophy

1.4.1 Introduction

Tau protein has been long known for its involvement in neurodegenerative disease [83], and, when it was discovered that the enzyme previously known as "Tau kinase 1" was in fact the GSK-3β [84], researchers started to uncover all the possible roles that "non-canonical" action of GSK-3 can play in pathology. Besides Tau phosphorylation, developmental roles, mitochondrial metabolism, or inflammation [85] have been discussed as possibly GSK-3-mediated means of pathological degeneration withing the central, peripheral nervous system and the connected skeletal muscle system. Notably, therapeutic targeting of GSK-3 has shown promises in the treatment of myotonic dystrophy (DM), a relatively (compared to diseases of similar nature) prevalent although scarcely studied [86] disease [87], [88]. Several recent reviews also discuss the important and complex function of Notch signaling in muscle health [89], [90], [91]. With inconclusive results of direct interaction between GSK-3 and Notch from the tissue cultures (**Table 1**) I thus focused my thesis further into testing if a link could be found in pathological process with cojoint involvement of GSK-3 and Notch receptor.

1.4.2 Myotonic dystrophy

Myotonic dystrophy is a genetic disease caused by two different forms (DM1 and DM2), both caused by expanded DNA tandem repeats, although each in a different gene. Myotonia describes the delay in one's ability to relax muscles after contraction [92]. Myotonia is considered a characteristic symptom of DM, but it can appear in other diagnoses as well [93]. DM1 is more severe and more common – it is the most diagnosed muscular dystrophy in adults.

The specific DNA regions affected are 3′ untranslated region of myotonic dystrophy protein kinase (DMPK) for DM1 and intron 1 of zinc finger protein 9 (ZNF9) for DM2 (reviewed on [94]). The fact that these repeats are outside of the protein-coding sections indicates that the primary molecular cause is on the level of DNA and RNA, rather than stemming from the DMPK and ZNF9 proteins themselves – the two are also not very similar in function. The expanded transcripts interfere with RNA-interacting proteins, resulting in increased amounts of CUGBP/Elav-like family member 1 (CELF1), a protein upregulated by GSK-3-mediated phosphorylation (reviewed in [95]). However, although RNA processing is implicated to be the core mechanism of DM pathogenesis, further supported by the promising efficiency of

targeting RNA pharmacologically [96], the impaired physiological processes are presumably mediated by diverse set of dysregulated proteins, as seen in some proteomic studies [97], [98]. In the following section, several physiological mechanisms relevant in neuromuscular health are reviewed from the perspective of their regulation by GSK-3 and Notch.

1.4.3 Pathophysiological mechanisms

Development and differentiation

Notch, as mentioned previously, regulates development of many different tissues, including nervous system, as well as musculoskeletal system [99].

The earliest phase of embryonic muscle development is the periodic formation of somites. These mesodermal structures will give rise to muscles, bones and vertebra, and represent a critical step in vertebrate embryogenesis [100]. The need for precise timing makes use of Notch signaling and its oscillatory capabilities. Notch, along with other pathways (mainly Wnt and FGF) give rise to the "segmentation clock" [101]. Canonical Notch signaling primarily blocks muscle differentiation and maintains muscle stem cell identity [99].

In post-embryonic development, muscle cells stem cells are referred to as satellite cells and are indispensable for muscle regeneration [95]. Notch, maintaining the pool of quiescent satellite cells [96], has been shown to become activated after muscle injury [97], as well as during puberty through the action of sex hormones [98]. GSK-3β inhibition also improves renewal and survival of satellite cells [99], while Wnt signaling effects on myogenesis seem to be dependent on the specific Wnt ligand isoform [102].

Although not nearly as large as in muscle, neural stem cell pool of homeostasis is also implicated in health [103], with Notch displaying comparable function as with their muscle counterparts [104].

Metabolism and mitochondrial dysfunction

Another characteristic shared by both muscle cells and neurons is their high energetic activity and dependence on mitochondrial function. GSK-3 has been shown to regulate multiple mitochondrial processes by phosphorylating various mitochondrial proteins, both on the membranes and inside, since small amounts of GSK-3β are present in mitochondria [105]. Notably, GSK-3β is an important regulator at the mitochondria-ER contact sites[106], where

its phosphorylation of VDAC affects the ER-mitochondria calcium exchange. VDAC proteins are also the key binding partners of hexokinase 2 (HK2) and this interaction allows for HK2's localization on mitochondria. The VDAC-HK2 complex formation is suppressed by phosphorylation, with GSK-3β being one of the dominant kinases in this process [107]. Hexokinase 2 is the catalysator of glucose (and to lesser extent also other hexoses) phosphorylation - the first step of carbohydrate catabolism, and its ratio between mitochondrial and cytoplasmic localization is an important way of regulation [108].

In the past years, Notch signaling was shown to play a role in the regulation of mitochondrial activity, both by canonical regulation of transcription [109], and by non-canonical extra-nuclear protein-protein interactions [110]. Notably, the relationship between Notch and mitochondrial membrane dynamics has been observed multiple times [110], [111], including the pathogenesis of muscle atrophy [112].

As evidence suggests, GSK-3 and Notch co-regulate a number of processes affected in neuromuscular disease. Understanding these pathophysiological mechanisms may help us uncover a more precise molecular context in which GSK-3 and NICD could potentially meet and perhaps provide insight into the elusive nature of their crosstalk.

Part 2: Goals

In my thesis I chose neurodegenerative and muscular disorders as the main topic and biological context. Due to the above stated role of GSK-3 and Notch and conflicting literature on their direct interaction I attempt to use insights from literature about their complex pathophysiology and select a potentially relevant protein interactor with both GSK-3 β and Notch 1.

- In silico analysis of proteomic data of GSK-3β-interacting proteins in DM patient muscle cells, provided by RNDr. Petr Novák, PhD
- Cloning with PCR amplification, restriction digest and ligation
- Optimizing the expression in HEK-293 cells
- Immunochemical experiments for possible interactions

Part 3: Materials and methods

3.1 Materials

3.1.1 Chemicals

Acrylamide/Bis-acrylamide	Sigma-Aldrich	A3574
Agarose Standard	ROTH	3810.2
Ammonium persulfate (APS)	Sigma-Aldrich	A3678
Ampicillin sodium salt	Sigma-Aldrich	A9518
Albumin bovine, Fraction V	SERVA	11930.03
Dimethyl sulfoxide (DMSO)	Sigma-Aldrich	D8418
Ethanol 96% (w/w)	Penta Chemicals	64-17-5
Ethylenediaminetetraacetic acid (EDTA)	Sigma-Aldrich	E5134
Formaldehyde 36% (w/w)	VWR	20909.290
Glycine	Penta Chemicals	56-40-6
Isopropyl alcohol	Penta Chemicals	17510-11000
Methanol A. G.	Penta Chemicals	67-56-1
N,N,N',N'-Tetramethyl-ethylenediamine (TEMED)	Sigma-Aldrich	T9281
Polyethylenimine, linear	Sigma-Aldrich	765090
Sodium chloride	Penta Chemicals	16610-31000
Sodium dodecylsulphate (SDS)	ROTH	S 19501
Tris(hydroxymethyl)aminomethane (Tris)	ROTH	2449.2
Triton X-100	Sigma-Aldrich	T8787
Tween® 20	Sigma-Aldrich	93773

3.1.2 Buffers

- Phosphate buffered saline (PBS)
    - PBS-T = PBS with 0.1 % (w/v)Triton 100
- Tris-acetate-EDTA (TAE)
- Tris buffered saline (TBS)
    - TBS-T = TBS with 0.1 % (w/v) Tween 20
- Tris-chloride buffers for polyacrylamide gels, pH 6.8, 8.8
- Running buffer for SDS-PAGE (Tris-glycine, 0.1 % (w/v) SDS, pH 8.3)
- Transfer buffer (Tris-glycine, 20 % (v/v) methanol, pH 8.3)
- Minipreparation buffers
    - P1 buffer (Tris-chloride buffer, 10 mM EDTA, 1 % (w/v) glucose, Rnase A, pH 8)
    - P2 buffer (0.2M sodium hydroxide, 1% (w/v) SDS)
    - P3 buffer (Potassium acetate buffer, pH 5)

3.1.3 Restriction enzymes

BamHI-HF	G/GATCC	New England Biolabs (NEB)	R3136
EcoRI-HF	G/AATTC	NEB	R3101
HindIII-HF	A/AGCTT	NEB	R3104
NotI-HF	GC/GGCCGC	NEB	R3189
XhoI	C/TCGAG	NEB	R0146

3.1.4 Antibodies

Donkey anti-Rabbit IgG (H+L) Highly Cross-Adsorbed Secondary Antibody, Alexa Fluor Plus 594 2 mg/ml	Invitrogen	A32754
Donkey anti-Mouse IgG (H+L) Highly Cross-Adsorbed Secondary Antibody, Alexa Fluor Plus 488 2 mg/ml	Invitrogen	A32766
Donkey anti-Rabbit IgG (H+L) Highly Cross-Adsorbed Secondary Antibody, Alexa Fluor Plus 488 2 mg/ml	Invitrogen	A32790

Goat Anti-Mouse IgG H&L (HRP) 2 mg/ml	Abcam	ab205719
Goat Anti-Rabbit IgG H&L (HRP) 2 mg/ml	Abcam	ab205718
Mouse Anti-Beta-Actin (C4) 0.2 mg/ml	Santa Cruz Biotechnology	sc-47778
Mouse HA tag antibody 0.5 mg/ml	GenScript	A01244S
Recombinant Anti-DDDDK tag antibody (Anti-FLAG) 0.675 mg/ml	Abcam	ab205606

3.1.5 Cloning enzymes

Q5 High-Fidelity DNA Polymerase Master mix	NEB	M0492S
Quick CIP (phosphatase)	NEB	M0525S
T4 DNA Ligase	NEB	M0202S

3.1.6 Commercial solutions

4× Laemmli Sample Buffer	Bio-Rad	1610747
DMEM, high glucose, GlutaMAX™ Supplement, pyruvate	Gibco	31966047
EliDNA PS Green	Elisabeth Pharmacon	ED01
Fetal Bovine Serum, qualified, Brazil	Gibco	10270106
Gel Loading Dye, Purple (6×)	NEB	B7024S
Gelatin solution, type B	Sigma-Aldrich	G1393-20ML
GeneRuler DNA Ladder Mix, ready to use	Thermo Fisher Scientific	SM0333
Lysogeny broth (LB) medium	IMG	--
MitoTracker™ Red CMXRos	Thermo Fisher Scientific	M7512
Mowiol® 4-88	Polysciences	17951-500
Opti-MEM™ I Reduced Serum Medium	Gibco	11058021
PageRuler Prestained Protein Ladder	Thermo Fisher Scientific	
Penicillin-Streptomycin (10,000 U/ml)	Gibco	15140122
Pierce™ ECL Western Blotting Substrate	Thermo Fisher Scientific	32209

Pierce™ Hoechst 33342 Solution (20 mM)	Thermo Fisher Scientific	62249
Pierce™ IP Lysis Buffer	Thermo Fisher Scientific	87787
Pierce™ RIPA Buffer	Thermo Fisher Scientific	89900
Plate ampicilin	IMG	--
Pierce™ Protease and Phosphatase Inhibitor	Thermo Fisher Scientific	PIERA32961
rCutSmart™ Buffer	NEB	B6004S
SuperSignal™ West Femto Maximum Sensitivity Substrate	Thermo Fisher Scientific	34096
Trypan Blue stain 0.4% (w/w)	Invitrogen	T10282
TrypLE™ Select Enzyme	Gibco	12563029

3.1.7 Kits

DNA Clean & Concentrator-5	Zymo Research	D4004
GeneJET Gel Extraction and DNA Cleanup Micro Kit	Thermo Fisher Scientific	K0831
GeneJET Plasmid Miniprep Kit	Thermo Fisher Scientific	K0502
Pierce™ BCA® Protein Assay Kits and Reagents	Thermo Fisher Scientific	23227

3.1.8 Cells

- HEK-293
- Escherichia coli, TOP10 Competent strain

3.1.9 Oligonucleotides

VDAC_F1	TGCAATGAGCGGCCGCATGTGTTCATTCTTTCTCGTGCTTTTG
VDAC_F2	AGTAGAATAAGAATTCCACTATCGCCACCATGGCCGTGCCTCCCACATAC
VDAC_R1	TTATTGACTCTCGAGTTACTTATCGTCGTCATCCTTGTAATCTGCTTGAAATTCCAGTCCTAG
VDAC_R2	TTATTGACTCTCGAGTTACTTATCGTCGTCATCCTTGTAATCTGCTTGAAATTCCAGTCCTAG
BGH_rev	TAGAAGGCACAGTCGAGG
T7_F	TAATACGACTCACTATAGGG

3.1.10 Vectors

- pBlueScript 2 (plasmid vector, not transcribed in eukaryotic systems)
- pcDNA3.1 (plasmid vector for mammalian expression)

- pcDNA3.1hNOTCH1-HA (codes for human NOTCH1 protein with a C-terminal hemagglutinin tag)
- pcDNA3.1hGSK3β-FLAG (codes for human GSK-3β protein with a C-terminal FLAG tag)
- pcDNA3.1hGSK3β-HA
- pcDNA3.1eGFP

3.1.11 Equipment

Models of equipment are specified in relevant parts of Methods section.

3.2 Methods

3.2.1 Proteomic data interpretation and potential target search

Filtered mass spectrometry data of proteins co-immunoprecipitated with GSK-3β from immortalized skeletal muscle cells of anonymized DM1 patients was provided by Dr. Petr Novák (Laboratory of Structural Biology and Cell Signaling at BIOCEV, currently unpublished). List of all protein IDs was analyzed, visualized and clustered using the internet-accessible tool String-db [113] and gene ontology analyzer g:Profiler [114] was queried with the proteins in separate clusters.

In the next part of the analysis, tool LFQ-Analyst [115] was used to compare the control and DM groups.

3.2.2 In silico protein-protein interaction and structure predictions

Alphafold2-multimer [116] was ran using the SpeedPPI/FoldDock protocol [117] to generate scored predictions of PPIs. Computational resources for Alphafold 2 predictions were provided by the e-INFRA CZ project (ID:90254). Later, Alphafold 3 was used on the same queries and additionally to predict structures involving phosphorylation (public server, [118]). Pymol [119] was used to visualize and evaluate outputs. Non-protein components in Alphafold 2 models were added using the AlphaFill tool [120], while Alphafold3 allows them without any additional tools.

3.2.3 Plasmid preparation

Primer design

FLAG-tagged mouse VDAC1 plasmid, along with a tag-less version, was cloned from cDNA. PCR primers were designed based on the Ensembl [121] canonical cDNA sequence of mouse VDAC1. Nucleotide BLAST [122] confirmed the lack of similar sequences. The overhangs included restriction sites for NotI (forward) and XhoI (reverse). Two variations of reverse primers were made, one with FLAG tag-coding sequence and one without.

PCR

Reaction mixture was prepared from following reagents: 12.5 µl of Q5 Hotstart Mastermix (2× concentrated), 2.5 µl of cDNA solution, 1.25 µl of VDAC_F1 and 1.25 µl of VDAC_R1 or VDAC_R2 primer, and 7.5 µl of nuclease-free water. PCR reaction was performed in Biometra TRIO Thermocycler with following setting:

Temperature (°C)	Time	Cycles
98	2:45 min	1
98	20 s	35
60	30 s	
72	35 s	
72	2 min	1

After PCR, the mixtures with NEB Gel Loading Dye Purple were loaded into 1.5 % agarose gels with EliDNA Green Dye (2.5 µl in Dye 50 ml TAE). Electrophoresis was performed at 90 V for 1 h. The amplicons of expected size were cut out and DNA was extracted using standard agarose gel extraction protocol for the NucleoSpin PCR DNA Cleanup Kit. Nanodrop One Spectrophotometer (Thermo Fisher Scientific, ND-ONE-W) was used to quantify the product. Resulting solution was additionally purified and concentrated with Zymo Research DNA Clean and Concentrator due to low purity.

Digestion with restriction endonucleases

The purified PCR products were mixed with 0.5 µl of both NotI and XhoI, 1.5 µl of rCutSmart buffer (10× concentrated) and diluted to 15 µl with nuclease free water. 1 µg of vector was mixed with 1 µl of both enzymes, 1.5 µl of rCutSmart buffer, 1 µl of QuickCIP phosphatase and diluted to 15 ul.

Mixtures were incubated at 37 °C for 1 h. They were separated on 1 % agarose gel electrophoresis at 90 V, and desired bands were cut out and extracted with NucleoSpin PCR DNA Cleanup Kit.

Ligation and transformation

Ligation mixtures were prepared with insert/vector stoichiometry of 2:1, aiming for total 17 fmol of vector. Separate ligation mixture was prepared from the remaining vector DNA without insert DNA, serving as self-ligation control. Mixtures composed of 2 µl 10× concentrated T4 ligase buffer, 1 µl T4 ligase, appropriate volumes of DNA extracts, and diluted to 20 µl with water. Each mixture was separated into different reaction, one was incubated at room temperature for 2 hours, one at 16 °C overnight (more effective according to ligase manufacturer).

Following the room temperature incubation, 5 µl of the solution was used for the transformation of 50 µl TOP10 competent bacteria. Bacteria were thawed and mixed with the DNA. Mixture sat on ice for 30 minutes, then a 45 second heat shock at 42 °C was performed before returning the mixture back on ice for 2 minutes. 200 µl of antibiotic-free LB medium was added to the mixture and bacteria expanded in a shaker (Eppendorf ThermoStat C; 37 °C, 600 RPM) for 1 h. 100 µl of this suspension was seeded on an ampicillin plate overnight at 37 °C. Identical process was performed for 5 µl of the control solution. Because of positive results, the solutions incubated at 16 °C were not used.

Miniprep

Five colonies (two transformed with non-tagged, three with tagged plasmid) were expanded overnight in 3 µl of LB with 100 µg/ul ampicillin, (37 °C; agitated at 250 RPM). Plasmid DNA was extracted from these cultures using alkaline lysis minipreparation protocol: Cultures were centrifuged in a table centrifuge at 13 000 g for 1 min, pellet was resuspended in 300 µl of P1 buffer, lysis of bacterial cells was performed by the addition of 300 µl of P2 buffer and incubation for 5 min at room temperature. Lysate was neutralized with 300 µl of P3 buffer and centrifuged at 13 000 g for 10 min. DNA was precipitated with 550 µl isopropanol, suspension centrifuged at 13 000 g for 10 min and resulting pellets washed with 250 µl ethanol. After all ethanol was dried, pellets were dissolved in nuclease free water.

Screening

Restriction digestion with EcoRI was used for validation of different clones, because VDAC1 insert contains an additional EcoRI restriction site and the vector contains another one, which means that restriction of positive clones should result in two DNA fragements. This was

performed for isolated plasmids of three clones for tagged and two for untagged variation. Reaction mixtures of 10 µl included 0.25 µl of EcoRI-HF, 1 µl of rCutSmart, 3 µl of minipreparated DNA solution and 5.75 µl of nuclease free water.

After 40 minutes of digestion at 37 °C, samples were analyzed with agarose gel electrophoresis (1 % agarose, 90 V, 40 min).

Sanger sequencing of positive clones was performed by DNA Sequencing Laboratory at BIOCEV, each clone was sequenced from two different primers, T7 and BGH_rev (opposite sides of insert). Received sequencing data was aligned and validated on Benchling.com.

Midiprep

Standard protocol for the GeneJET Plasmid Miniprep Kit for low-speed centrifuge (<4000 g) was used to yield 350 µl solutions of isolated plasmid DNA, which was stored at -17 °C.

Reinsertion

The protein-coding sequence of the final tagged plasmid was later reinserted into pcDNA3.1 because of a suspected mutation in non-coding regions. Reaction mixtures of total volume of 15 µl were prepared with 1 µg of both the plasmid and vector, 1 µl of BamHI-HF and XhoI, 1.5 µl of rCutSmart buffer concentrate. 1 µl of CIP was added to the pcDNA3.1 mixture.

After 1 h of incubation at 37 °C, separation was performed using agarose gel electrophoresis (1 %, 90 V, 40 min). The shorter fragment of the plasmid and the only visible product of pcDNA3.1 were extracted with NucleoSpin PCR DNA Cleanup Kit. Ligation, transformation, selection of clones and isolation were done same way as previously.

3.2.4 Expression in HEK

Cell culture maintenance

A vial of HEK-293T Cells was thawed, seeded in DMEM medium with 1 % (v/v) penicillin-streptomycin (stock solution), 10 % (v/v) fetal bovine serum (hereinafter referred to as DMEM Complete) and incubated in CO_2 incubator at 37 °C for 48 h. Light microscope was used to monitor confluency. Cells were split into 6 well plates 18-24 hours before transfection.

Transfection for WB

Transfection was performed the day after seeding, with the intention to transfect at around 80 % confluency. mVDAC1-FLAG was transfected, along with eGFP-pcDNA3.1, which served as a control of transfection efficiency.

PEI was mixed with 50 µl of OptiMEM and incubated at room temperature for 15 minutes. This mixture was added to the solution of desired plasmids, also diluted in 50 µl of Optimem. The ratio of PEI:DNA was 3 µl of working solution for 1 µg of plasmid DNA. Total amount of 2 µg DNA was usually used for a single well (6-well plates, 9.6 cm^2). The final transfection mixture was incubated for 20 minutes and added to cells in drop-wise manner.

Transfections with different lipid-based commercial reagents were also attempted, but with lower efficiency than PEI.

Several hours (3 – 6) after transfection, media were changed. At least 24 hours post-transfection, cells were lysed with RIPA buffer + protease/phosphatase inhibitor cocktail and lysates were collected into 1.5 ml tubes.

SDS PAGE

BCA protein assay kit was used to determine protein concentrations in the lysates; 10 µl of BSA standards (dissolved in RIPA buffer at concentrations of 2000, 1000, 500, 250, 125, 25 µg/ml) and 10x diluted lysates were added to the reagent, incubated at 37 °C for 1 hour and Artel BioTek ELX800NBART Microplate Reader was used to measure absorbance at 562 nm. Relevation DSX software generated calibration curve and the protein concentrations of lysates. Samples of consistent protein concentrations were prepared by diluting lysates i accordingly and mixing with appropriate volume of 4x concentrated Laemmli buffer. Based on the measured concentration samples were diluted in RIPA buffer to reach a uniform concentration of 1.25 µg/ul (20 ul loading volume would contain 25 µg of total protein). The samples were denatured at 98 °C for 5-10 minutes.

12 % polyacrylamide gels were prepared from 3.75 ml 1.5 M Tris-Cl buffer (8.8 pH), 5 ml H_2O, 75 µl 20 % (w/v) SDS, 6 µl 30 % (w/v) acrylamide/bisacrylamide, 7.5 µl TEMED and 35 µl APS per one gel and casted in Bio-Rad MiniPROTEAN system. Stacking was made of 2.5 ml H_2O 0.8 ml 30 % acrylamide/bisacrylamide, 0.5 ml 1 M tris-Cl (6.8 pH), 20 µl 20 % (w/v) SDS, 5 µl of TEMED and 35 µl 10 % (w/v) APS.

Wells were loaded with 3 µl of pre-stained protein ladder and 20 µl of prepared samples Electrophoresis was performed in running buffer at 90 V. Line formed by bromophenol-blue

(contained in Laemmli) was used to monitor progression. The voltage was increased to 130 V after samples left the stacking gel.

Western blot

TransBlot Turbo system was used to transfer protein from the gel to a PVDF membrane. The parameters were set as: 25 V, 2.5 A and 15 minutes. Membrane with transferred proteins was blocked in 10 % (w/v) non-fat milk in TBS-T buffer for 1 hour and then incubated with anti-FLAG antibody (diluted 1:1000 in TBS-T with 1 % (w/v) BSA) overnight at 4 °C. Membrane was washed 3 times with TBS-T and incubated with anti-rabbit HRP-conjugated secondary antibody (1:2000, TBS-T with 1 % BSA). After washing the membrane 3 times, membrane was incubated with ECL substrate solutions for 5 minutes and chemiluminescence was detected using ChemiDoc Imaging System (Bio-Rad, 12003153). Later, the antibody incubation process was repeated but with anti-beta-actin primary antibody (mouse) and anti-mouse secondary antibody.

3.2.5 Immunocytochemistry

Cell seeding for immunofluorescent sample preparation

Sterilized coverslips were inserted in the wells of 24 well plate, coated in 0.1 % (w/w) gelatin for 20 minutes, after which gelatin was aspirated and coverslips dried at room temperature.

HEK-293T cells were grown for 2 days in a 10 cm plate. After that, cells were detached using TrypLE and suspended in medium. Automatic cell counter was used to calculate the number of cells. Suspension was centrifuged at low speed for 3 minutes and the pellet was diluted in DMEM Complete to a concentration of 600 cells/µl and 100 µl (60 000 cells) was added to each of 10 wells containing coated coverslips and 600 µl of DMEM Complete.

Transfection

After 24 h from seeding, transfection was performed. 12 µl PEI (equivalent to final ratio of 3 µl PEI per 1 µg DNA) was incubated in 500 µl Optimem for 20 minutes. Plasmid mixtures according to **Table 2** were diluted each in 50 µl of Optimem. 50 µl of the PEI solution was added to each DNA mixture which was incubated for 20 minutes. The 100 µl mixtures were carefully dropped in each well. After 3.5 hours, the PEI-containing medium was replaced with fresh pre-heated DMEM Complete.

Mitotracker

The Mitotracker solution was prepared by mixing 0.5 µl of 1 mM Mitotracker in DMSO and 5 ml serum free medium to yield final concentration of 100 nM. 24 hours post transfection, medium of the indicated samples (see **Table 2**) was replaced with 500 µl of the 100 nM Mitotracker solution and cells were incubated at 37 °C for 30 minutes.

Fixing and blocking

Medium was aspirated and cells were rinsed once with PBS followed by addition of 200 µl 4 % formaldehyde for 15 minutes in room temperature. Fixing solution was then removed and cells washed 3 times with PBS-T.

Non-specific binding of the primary antibody was prevented by 45 min incubation in 3 % BSA in PBS-T at RT.

Primary antibody incubation

Three solutions were prepared by diluting primary antibodies in PBS-T with 3 % BSA – anti-FLAG (diluted 1:100), anti-HA (at 1:500) and a solution containing both antibodies at same total dilution. 200 µl of the appropriate solution (see **Table 2**) was added to each well. The plate was then incubated overnight at 4 °C.

Secondary antibody incubation and mounting

Cells were washed with PBS-T for 10 min three times and then incubated for 1 hour at room temperature in 200µl solutions of Alexa Fluor-conjugated secondary antibodies. Three different antibodies were used – donkey anti-mouse Alexa Fluor 488, donkey anti-rabbit Alexa Fluor 488 and 594. Stock solutions of both 488-conjugated antibodies were diluted 1:2000, while the 594 was diluted 1:1000 in PBS-T.

Secondary antibodies were removed, and wells were washed in PBS-T 3 times. After the last wash, PBS-T was replaced with 0.1 µg/ml solution of Hoechst 33342 in PBS and incubated at room temperature for 20 minutes. Wells were washed with PBS. Microscope glass slides were cleaned with ethanol. Each cells-containing coverslip was removed from its well and placed onto the microscopy glass slide with 20 µl Mowiol between the slide and the cell-covered side of coverslip.

Table 2: All prepared samples for immunocytochemistry with plasmids used in transfection and antibodies/Mitotracker added. AF – AlexaFluor.

Plasmid / Sample	pcDNA3.1hNOTCH1-HA	pcDNA3.1hGSK3β-FLAG	pcDNA3.1hGSK3β-HA	pcDNA3.1mVDAC1-FLAG	pcDNA3.1	pBlueScript 2	**Mitotracker**	**Primary antibodies**	**Secondary antibodies**
Control	-	-	-	-	150 ng	250 ng	+		Anti-Mouse, AF 488
Notch1+Mito	50 ng	-	-	-	100 ng	250 ng	+	anti-HA	Anti-Mouse, AF 488
GSK3B+Mito	-	50 ng	-	-	100 ng	250 ng	+	anti-FLAG	Anti-Rabbit, AF 488
VDAC1+Mito	-	-	-	50 ng	100 ng	250 ng	+	anti-FLAG	Anti-Rabbit, AF 488
Notch1+GSK3B	50 ng	50 ng	-	-	-	250 ng	-	anti-FLAG, anti-HA	Anti-Rabbit, AF 594 + Anti-Mouse, AF 488
Notch1+VDAC1	50 ng	-	-	50 ng	50 ng	250 ng	-	anti-FLAG, anti-HA	Anti-Rabbit, AF 594 + Anti-Mouse, AF 488
Notch1+Mito with GSK3B and VDAC1 overexpression	50 ng	50 ng	-	50 ng	-	250 ng	+	anti-HA	Anti-Mouse, AF 488
GSK3B+VDAC1	-	-	50 ng	50 ng	50 ng	250 ng	-	anti-FLAG, anti-HA	Anti-Rabbit, AF 594 + Anti-Mouse, AF 488
GSK3B+Mito with N1 overexpression	50 ng	50 ng	-	-	50 ng	250 ng	+	anti-FLAG,	Anti-Rabbit, AF 488
VDAC1+Mito with N1 overexpression	50 ng	-	-	50 ng	50 ng	250 ng	+	anti-FLAG,	Anti-Rabbit, AF 488

3.2.6 Fluorescence microscopy and image analysis

For the analysis of stained cells, widefield fluorescent microscope Leica DMi8 was used. For initial observations, objective 10x was used, for image acquisition the objectives 20x and 40x. All objectives were "dry" - without immersion liquid. LAS X software was used to optimize exposure settings, capture, export images and scalebar.

3.2.7 Immunoprecipitation of HA-tagged Notch1 in HEK-293T

Cell cultures

HEK-293T cells were used for the experiment. 18 hours prior to transfection, 1.2 million cells per plate were passaged to 4x 10cm plates with DMEM Complete and expanded in the incubator overnight.

Transfection

Each plate was transfected with 5 µg DNA using PEI (ratio kept as previously mentioned). The control plate was transfected with 2.5 µg pcDNA3.1 and 2.5 µg pcDNA3.1eGFP, two samples were transfected with 2.5 µg pcDNA3.1 and 2.5 µg of a single plasmid, and last sample included 2.5 µg of both pcDNA3.1hNOTCH1-HA and pcDNA3.1mVDAC1-FLAG plasmids.

Cells were incubated for 5 hours after which the medium was replaced. Transfection efficiency was confirmed with GFP fluorescence of control.

Immunoprecipitation

Cells were incubated until 24 h from their transfection. Then, media were aspirated, cells were washed with cold PBS and lysed in 4 °C for 20 minutes using 1 ml of CoIP Lysis buffer + protease/phosphatase inhibitor cocktail. Lysates were scraped into 1,5 ml tubes and centrifuged in 4 °C at maximal speed (14 000 g, swing-bucket rotor) for 15 minutes. Two samples of 400 µl from each tube were collected, along with separate 60 ul/sample later used as total lysate reference. The 400 µl of protein solutions were incubated with 2,5 µl of antibody for 1 h at 4 °C. For each lysate, one sample was incubated with mouse anti-HA antibody and one with control mouse IgG. Sepharose G protein beads were washed with CoIP lysis buffer and 40 µl of bead suspension was added to each sample. Following overnight incubation at 4 °C, beads were purified by washing with PBS, centrifuging at 4 °C (0.1 g, 1 min) and removing the supernatant (3x repeated). Beads were then diluted in 42 µl of 2×

concentrated Laemmli buffer and boiled for 5 minutes at 95 °C. The total cell lysate samples were diluted with 15 µl of 4× concentrated Laemmli and boiled for 5 minutes at 95 °C.

Western blot

12 % polyacrilamide gel was prepared and 20 µl of following samples were loaded, along with 2× 5 µl of pre stained ladder: HA-precipitate sample per each (4×), IgG precipitates of cells transfected with pcDNA3.1mVDAC1-FLAG and co-transfected with pcDNA3.1mVDAC1-FLAG + pcDNA3.1hNOTCH1-HA (2×), and the corresponding total cell lysates. SDS-PAGE ran at 100 V, later increased to 115 V. Proteins were transferred to PVDF membrane with TransBlot Turbo system (25 V, 2.5 A, 15 min). Membrane was blocked with 10 % non-fat milk in TBS-T for 1 h at room temperature and then incubated with primary antibodies (anti-FLAG, anti-HA, 1:1000 dilution in TBST with 1 % (w/v) BSA) overnight at 4 °C. Membrane was washed with TBST and incubated with secondary antibodies (HRP conjugated, 1:20000 dilution in TBST with 1 % (w/v) BSA) for 1 h at room temperature. Membrane was washed in TBST and incubated for ~5 minutes with ECL substrate. Chemiluminescence was measured with Chemidoc.

3.2.8 Optimizing VDAC1 expression in HEK cells

HEK-293T cells in the quantities of 50 000 were seeded in a 24-well plate with DMEM Complete and incubated overnight. Transfection with PEI followed the same general protocol as previously with amounts of 20, 50, 100, 200, 300 ng of either pcDNA3.1hGSK3β-FLAG or pcDNA3.1mVDAC1-FLAG and pBluescript2 adding up to 500 ng per well. Medium was changed after 4 hours. Cells were lysed and harvested after 36 hours, lysates were quantified, and samples were prepared by mixing lysates with appropriate volume of RIPA buffer and 4× concentrated Laemmli to final protein concentration of 750 ng/ul (15 µg in 20 µl). Samples were denatured as described previously. SDS-PAGE/Western blot protocol was also identical to previous VDAC1 expression experiments, except for the addition of FemtoWest peroxidase substrate to visualize low-concentration proteins.

Part 4: Results

4.1 In silico prediction of glycogen synthase kinase 3 beta and Notch 1 intracellular domain interactions

I used several *in silico* approaches to model possible interactions between GSK-3B and N1ICD. AlphaFold2-based protocol SpeedPPI was queried with amino acid sequences and generated interaction predictions. The models with full-length NICD possibly indicate involvement of the residue Thr-1898. This threonine has not been experimentally shown as a substrate of GSK-3. However, it has been shown to be phosphorylated following the phosphorylation of Ser-1901 by casein kinase 2 [123], a common priming kinase for GSK-3.

The full length NICD includes highly disordered regions so the following predictions were done only with parts of NICD. Fragments C-terminally of the ankyrin repeats produced low-confidence results with few-to-no secondary structures. Ankyrin repeats, despite having large interface for PPIs, did not seem to contain any Ser/Thr that could be properly oriented towards the GSK-3 binding pockets. The N-terminal part of N1ICD was involved in the intriguing complexes, based on the proximity between Ser/Thr and GSK-3 catalytic site. Thr-1861, reported as a GSK-3 target (**Fig. 5A, Fig. 5A,B**), appeared to interact with the primed phosphate binding site rather than the catalytic center itself. As Alphafold 2 uses only the 20 canonical amino acids with no modifications, its predicted models have no phosphorylated residues. Manually adding phosphate to Thr-1861 created a model resembling primed phosphate binding to GSK-3β (**Fig. 5B**). Although nearby Ser-1856 would seem like the expected target, the active site was occupied by a different part of N1ICD with closest Ser/Thr being Ser-1791 (**Fig. 5C,D**). Unlike Ser-1856, Ser-1791 has been reported to be phosphorylated in phospho-proteomic studies [124]. The RBP-Jκ/CBF1-associated module (RAM), which contains Ser-1791, is linked by a flexible disordered sequence and known to interact allosterically with CSL [125], [126].

Predictions using the recently introduced Alphafold 3 [118] can expand on these ideas. With the option to specify PTMs and cofactors, kinase model prediction is more reliable. Alphafold produced models with Ser-1791 in the proximity of GSK-3β's catalytic site, while phosphorylation of Thr-1861 caused interaction trough the binding pocket and displaced the

RAM domain. The possible structures of GSK-3β phosphorylating reported residues in the NLS were still low in confidence (**Fig. 5E**).

These predictions are in no way accurate representations of the nature of this interaction but show Ser-1791 as a possible target of GSK-3β and propose the role of other PTMs, as well as competition between different N1ICD sites, in influencing the outcome of its phosphorylation. As such, a hypothetical mediator could regulate the interaction for example by binding different NICD domains.

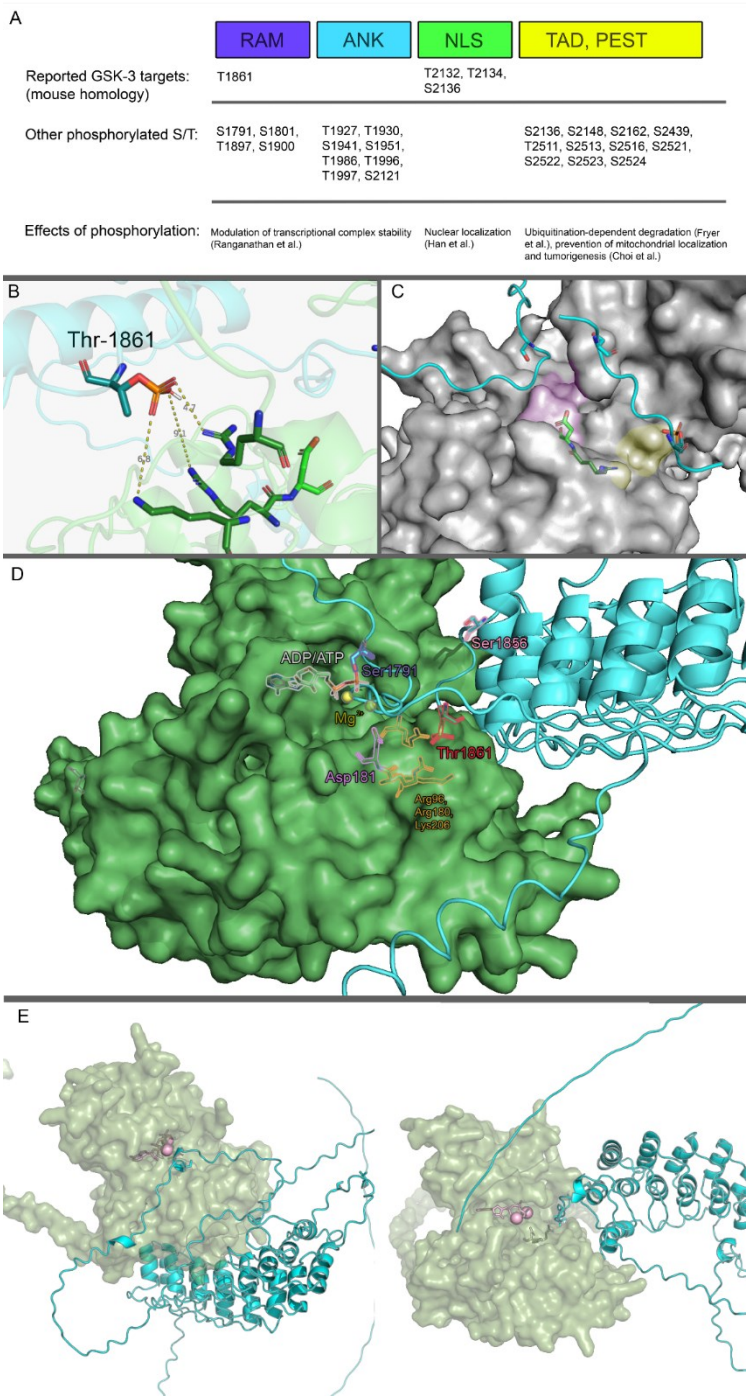

Fig. 5: In silico modelling of GSK-3β interaction with N1ICD. A: Scheme of N1ICD and a list of Ser/Thr residues either directly reported as GSK-3 targets or listed as in PhosphoSitePlus database [150], [151], [152], [153], [154]. NICD has another NLS sequence, C-terminal to ANK, not shown in the scheme. B: N-terminal fragment of N1ICD (cyan) in predicted interaction with GSK-3β's binding site (green). C: GSK-3β surface with approximate locations of the active site (pink) and binding site (yellow). The two cyan strands are regions of N1ICD containing Ser-1791 (left) and Thr-1861 (right). D: Full model of predicted GSK-3β (green) and N1ICD (cyan) showing both Ser-1791 interacting with the active site and phosphorylated Thr-1861 in the binding pocket. Predicted model was manually extended with ankyrin repeats using alignment with different model. E: Models predicted with Alphafold3 with no PTMs (left) and phosphorylated Thr-1861 (right).

4.2 Characterization of GSK-3B interactome

Dataset provided by Petr Novák, representing statistically significant interactors of GSK-3β from immortalized muscle cell lines isolated from patients with DM1 included 87 proteins. Gene ontology tools and String-db generation of functional protein network successfully provided basic overview of the interactome.

The change of individual proteins' quantities between control and patient cells is a way to predict their pathological relevance. Generated quantitative results indicate that proteins that are the most significantly downregulated are (based on p value) TNNI1 (troponin I 1), WFS1 (wolframin) and RAB1B (Ras-related protein-1B), and downregulated FN1 (fibronectin), PPHLN1 (periphilin 1), RPL12 (ribosomal protein L12). These results are plotted on a volcano plot (**Fig. 6**).

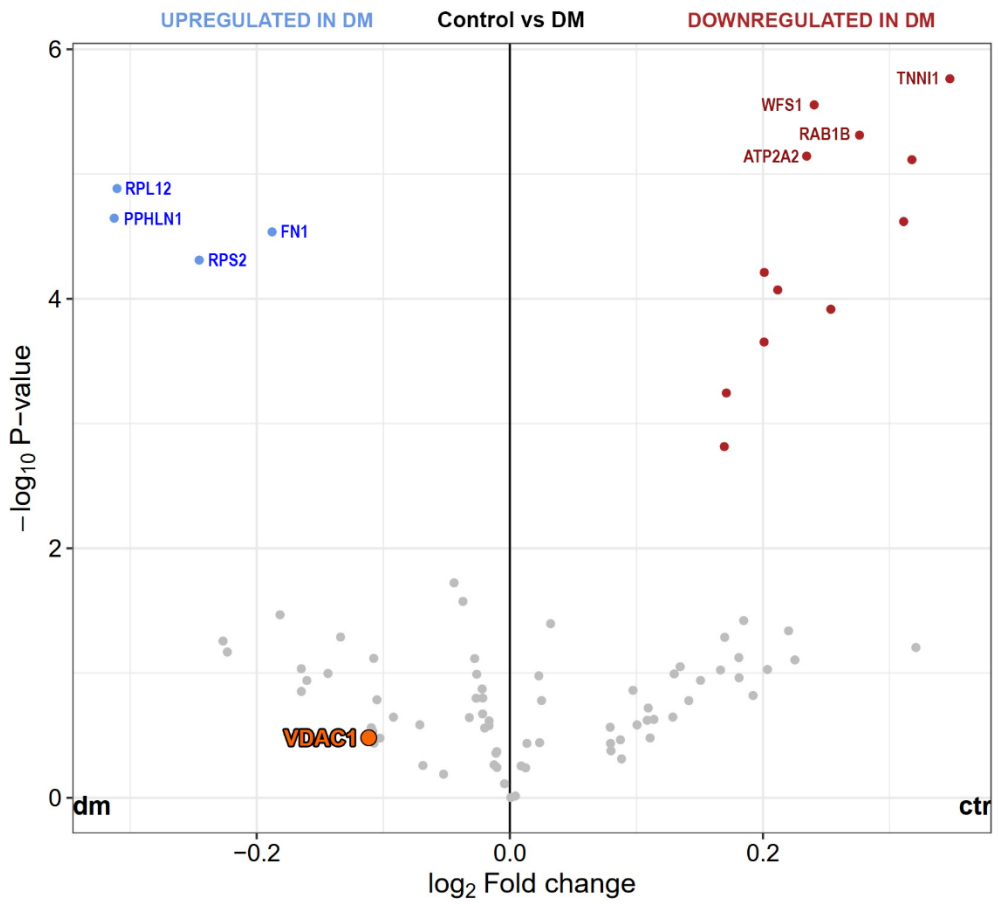

Fig. 6: Volcano plot. Fold change of label-free quantity measured in control samples in comparison to DM. Colored dots represent the proteins with $p < 0.05$ and $|\log_2 FC| > 0.1$, and the four upregulated and downregulated proteins with highest significance are marked with their abbreviated names. Selected protein, VDAC1, was on avarege slightly higher in DM samples, but this difference is not significant.

We couldn’t find any plausible link between the GSK-3β and Notch using these top candidates and we thus employed StringDB to uncover deregulated processes, which would point at candidate target facilitating Notch-GSK3 interaction. The resulting protein network could be divided into 3 functional clusters – 1. nuclear or nucleic acid-interacting proteins, 2. proteins of mitochondria, ER, Golgi apparatus and vesicles and 3. proteins of cytosol, membrane, and ECM. Prevalent gene ontology terms for the different clusters included various RNA-related processes for nuclear, striated muscle contraction and structure for compartmented, and axon and cytoskeleton for cytosolic.

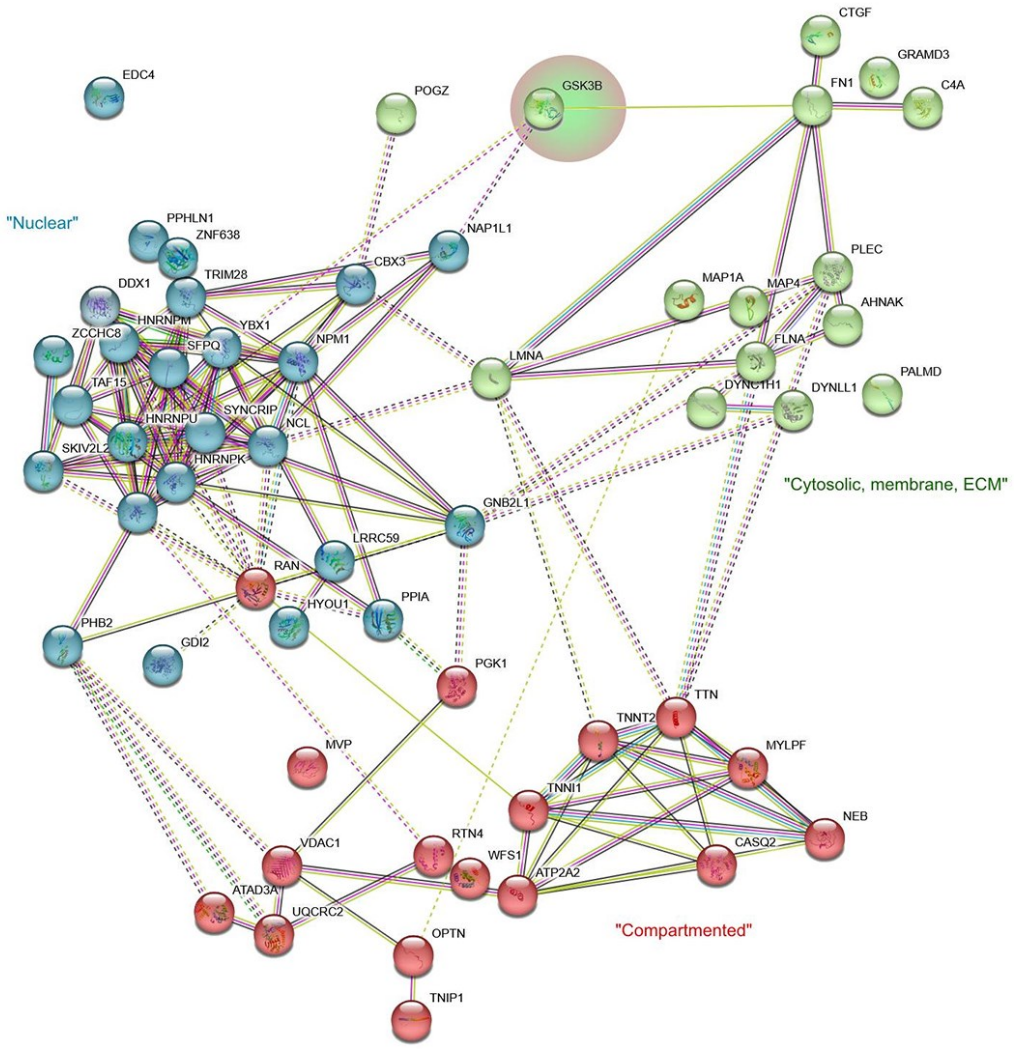

Fig. 7: StringDB-generated network. Proteins from MS data were clustered and interlinked using StringDB. The network is missing ribosomal proteins, histones and chaperones involved in folding, as they were removed due to large numbers of interactions.

Table 3: Top gene ontology terms for individual clusters, as determined by gProfiler. The order was based on adjusted p value which considers the number of positive proteins in a cluster against total in database. Used sources for terms: GO molecular function, GO cellular component, GO biological process, KEGG, Reactome, Wikipathways.

	Term	p value	Term	p value	Term	p value
1.	Striated Muscle Contraction	4.20×10^{-05}	axon	7.02×10^{-08}	RNA binding	3.08×10^{-09}
2.	Striated muscle contraction pathway	4.55×10^{-05}	neuron projection	6.40×10^{-07}	organelle lumen	3.18×10^{-08}
3.	sarcomere	5.20×10^{-05}	supramolecular fiber	2.92×10^{-06}	intracellular organelle lumen	3.18×10^{-08}
4.	Muscle contraction	5.37×10^{-05}	supramolecular polymer	3.09×10^{-06}	membran×10-enclosed lumen	3.18×10^{-08}
5.	cardiac muscle contraction	5.80×10^{-05}	polymeric cytoskeletal fiber	1.29×10^{-05}	mRNA binding	9.56×10^{-07}
6.	striated muscle thin filament	7.61×10^{-05}	supramolecular complex	3.05×10^{-05}	spliceosomal complex	7.28×10^{-06}
7.	myofibril	8.33×10^{-05}	plasma membrane bounded cell projection	6.74×10^{-05}	mRNA processing	9.39×10^{-06}
8.	contractile fiber	1.02×10^{-04}	dendrite	7.57×10^{-05}	nucleoplasm	1.27×10^{-05}
9.	myofilament	1.26×10^{-04}	dendritic tree	7.71×10^{-05}	Large Drosha complex	1.73×10^{-05}
10.	striated muscle contraction	2.58×10^{-04}	cell projection	1.02×10^{-04}	cytoplasmic ribonucleoprotein granule	2.58×10^{-05}
	Compartmented		*Cytosol*		*Nuclear*	

Particularly interesting region was mitochondrial and ER/SR proteins, such as voltage-gated anion channel 1 (VDAC1) or SR/ER calcium ATPase 2 (ATP2A2), with the top gene ontology terms being muscle related. Although StringDB-generated network didn't show a direct link between VDAC1, ATP2A2 and GSK-3β, both proteins were shown to be direct interactors [106], [107], [127]. VDAC1 was chosen for further experiments because of its relevance in disease, established link with GSK-3 and recent advances in the research of Notch's role in mitochondria and muscle dystrophy [112], including a possible PPI with VDAC1 [128].

4.3 Cloning of VDAC1 plasmid

To test interactions of VDAC1 experimentally I first needed to prepare an expression vector carrying its sequence. Because of high conservation of VDAC1 between mouse and human (**Fig. 8**), PCR was used to amplify protein-coding mVDAC1 sequence from an available sample of mouse cDNA. PCR also served the purpose to add FLAG tag (DYKDDDDK); a non-tagged variation was produced alongside. This step yielded an amplicon of expected size (around 900 bp) for both variations, as confirmed by agarose electrophoresis. Restriction digest was analyzed on agarose electrophoresis as well, but due to small difference between input and expected product, the success couldn't be determined confidently. The yields had been low, barely enough to prepare the 17 fmol ligation mixture (corresponding to 56.78 ng of total vector DNA, ca. 19.4 ng of insert).

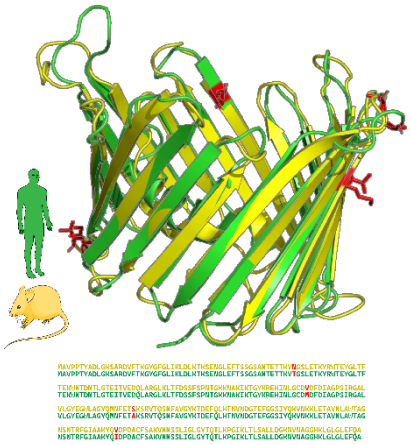

Fig. 8: The conservation of VDAC1 in mouse and human. Differing residues are highlighted in red. Structures from PDB – 3EMN (mouse) [155], 5XDO (human) [156].

Vector/insert ligate transformed bacteria grew desirable number of ampicillin-resistant colonies, as opposed to the vector self-ligation control which didn't grow any colonies.

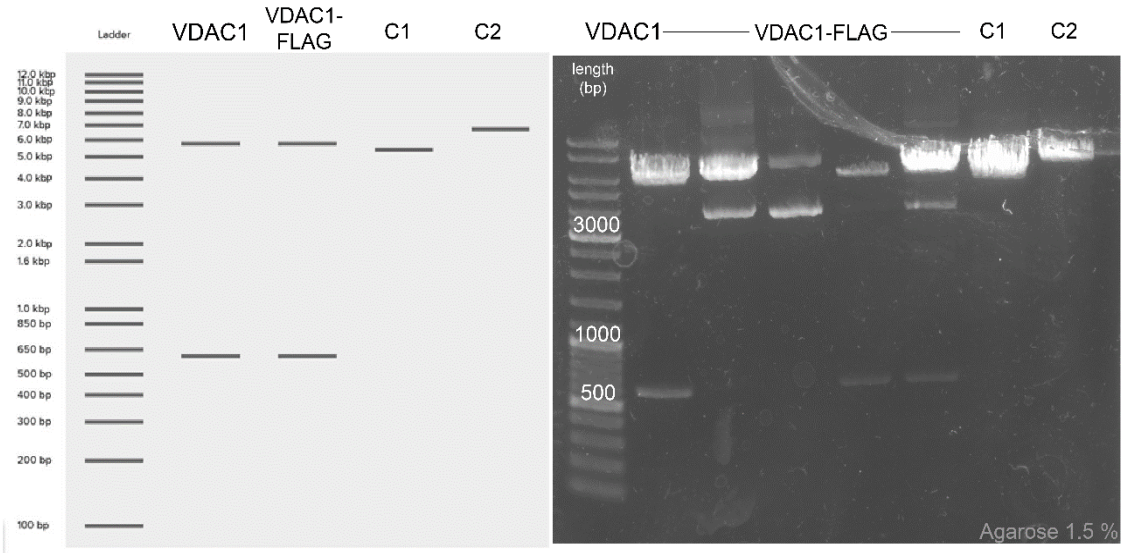

Fig. 9: Original screening of plasmid clones digested by EcoRI. Left side shows Benchling-generated virtual digestion of both cloned plasmid variants, controls C1 (empty pcDNA3.1 vector) and C2 (pcDNA3.1hGSK-3β plasmid). Right image shows the actual results after agarose electrophoresis.

Restriction screening produced expected bands of sizes around 6000 and 600 bp (**Fig. 9**), and two colonies (one for each variant) were selected and sent for Sanger sequencing.

Sequencing confirmed the correct sequence for the non-tagged clone but showed a single point mutation (162W>stop) for the selected FLAG-tagged one. Different tagged clone was later sequenced, and the correct sequence and orientation of insert was determined. This plasmid was used for following experiments, but consistently showed suboptimal expression (as described in the next section). The insert sequence was later excised and ligated into a new pcDNA3.1 vector. However, this step didn't significantly improve its expression.

4.4 Expression in HEK-293T

The cloned pcDNA3.1mVDAC1-FLAG has been transiently transfected and validated multiple times, consistently showing low expression and "double band" appearance on western blot. Linear PEI was concluded to be the most effective transfection reagent and different alternatives were not used further (see Chyba! Nenalezen zdroj odkazů.).

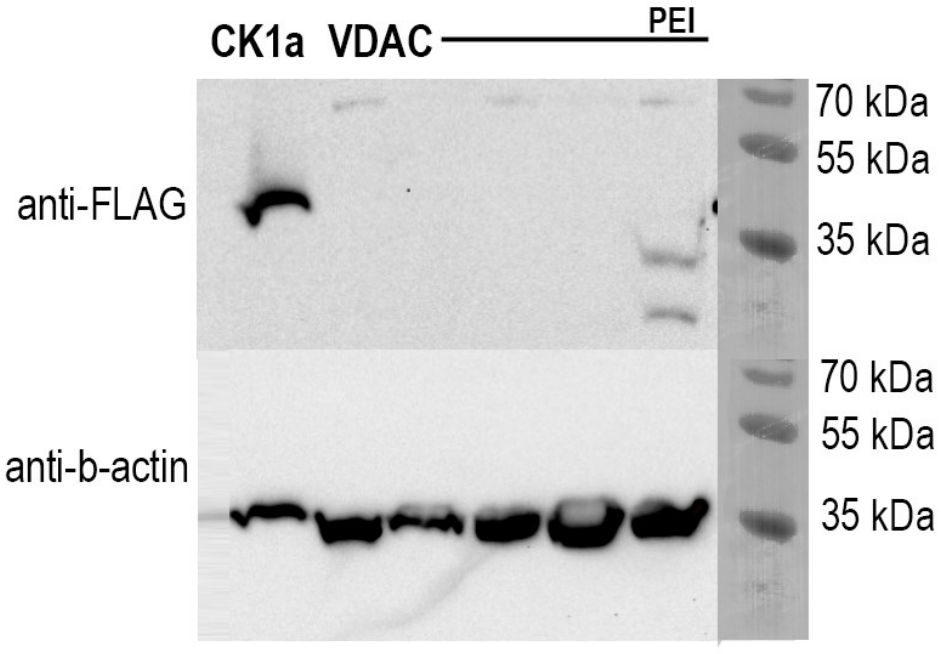

Fig. 10: Western blot of first VDAC1 expression in HEK-293T. CK1a serves as a positive control for FLAG antibody. With ECL substrate, VDAC1 could be detected only in the sample with PEI used as a transfection reagent. Other reagents used, with no visible bands in the image, were: Mirus Bio™ TransIT™-LT1, GenJet™ In Vitro DNA Transfection Reagent, FugENE HD Transfection Reagent, Lipofectamine 2K.

Detecting VDAC1 at correct size and assuming that the lack of expression in other samples was due to inefficient reagents or inadequate protocol, the plasmid and PEI were used for other experiments. However, it later became clear that the expression was very low, and the plasmid needed to be optimized to perform less sensitive PPI experiments, such as co-immunoprecipitation. Multiple western blot experiments were performed, yielding consistent results, with other plasmids in same vector and promoter being expressed much more effectively.

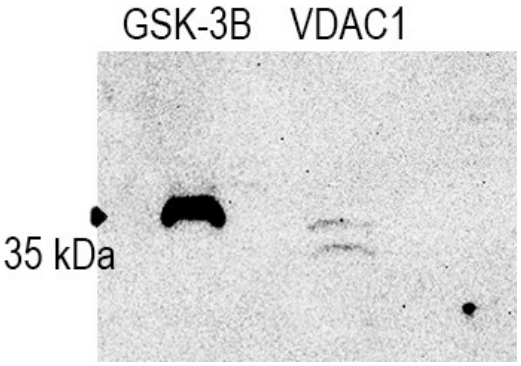

Fig. 11: An example of replicated WB experiment. Samples transfected with 10 µg plasmids and grown in 10cm plates were lysed and detected for FLAG (both proteins are FLAG-tagged).

4.5 Optimizing mVDAC1 expression in HEK cell lines

To test if the overexpression is toxic to the cells or induces a different dose-dependent response, cells were transfected with varying amounts of pcDNA3.1mVDAC1-FLAG and pcDNA3.1hGSK3β, and the lysates were compared on western blot. However, contrary to our hypothesis, differences between both protein's intensities were very apparent in all samples. The first scan with only ECL substrate showed 300 and 200 ng samples of GSK-3β as saturated while only the 300ng sample of VDAC1 could be detected. After applying FemtoWest, the other VDAC1 samples were revealed without any noticeable non-linear relationship to the transfected plasmid amount.

Detection of beta-actin in the same blot confirmed that the samples were of approximately equal sizes. Adjusted volume of 100 ng GSK-3β band (the highest non-saturated on ECL scan) and 300 µg VDAC1 band (the only visible on ECL scan) results and normalizing per plasmid mass results in the ratio of GSK-3β:VDAC1 (all three visible bands combined) of around 14. Assuming complete linearity, this would mean that the amount of transfected VDAC plasmid would need to be 14 times higher for them to have the same intensity.

VDAC1 signal appeared in three separate bands of sizes 33.7, 36.8, 39.6 kDa (from ImageLab MW tool). The protein coded by my plasmid has theoretical MW of 33 346 Da (expasy.org, ProtParam [129]). The two additional bands were detected around 3 and 6 kDa above the presumed intact protein, which would indicate addition of PTMs rather than proteolysis (that would result in bands below expected size). However, western blot is not a

precise method for determining molecular weight and in previous experiments, only 2 defined bands were observed, making this result an outlier.

After closer inspections of different VDAC1 protein sequences, I realized that the canonical mouse VDAC1, which the cloning primers were based on, is a less usual splice variant, referred to as pl-VDAC1, which has been reported only in mice (reviewed in [130]). The variant contains an additional N-terminal sequence with MW around 1.6 kDa (ProtParam), which would correspond to the spacing between bands more than common PTMs.

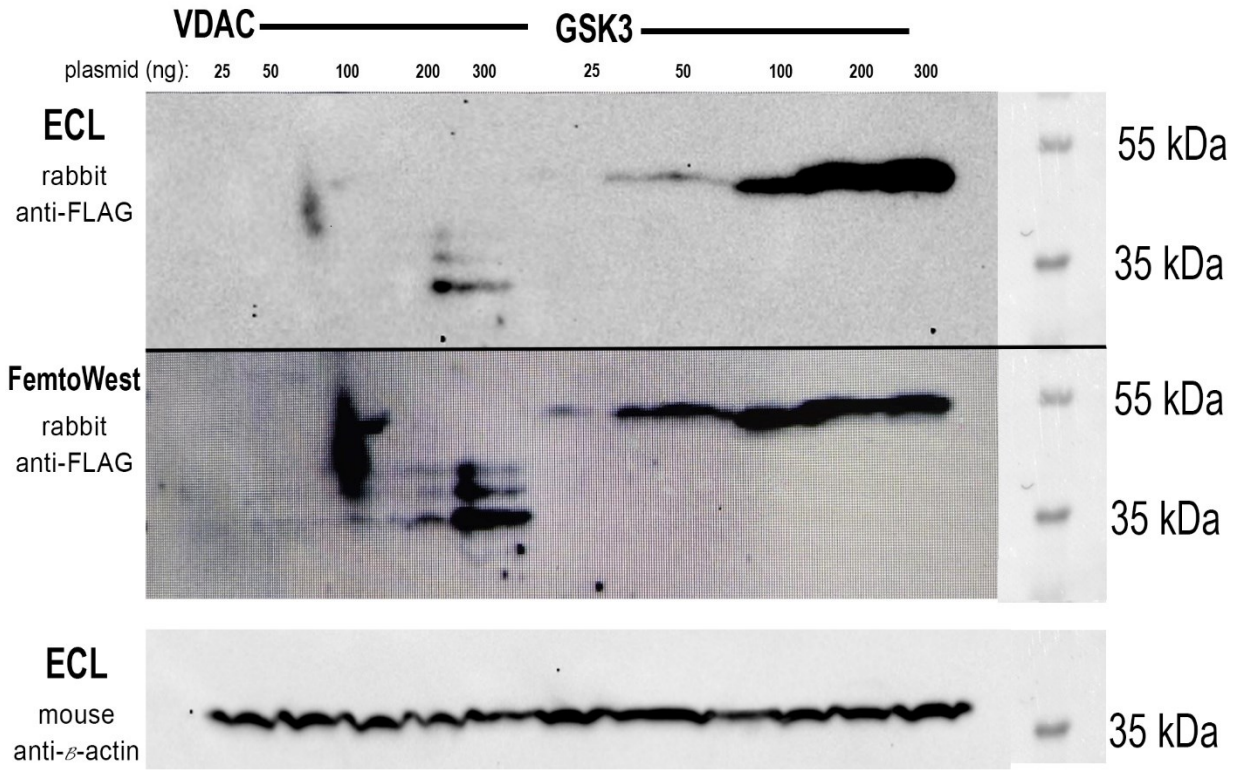

Fig. 12: Western blot showing the dependence of transfected plasmid amount on expression of VDAC1 vs GSK-3 (control). VDAC1 expression is much lower than GSK-3 and this apparent difference occurs at any transfected amount. β-actin was used as a loading control. (Original, high-quality, Chemidoc files of the FemtoWest scan have been lost)

4.6 **Immunocytochemistry**

HEK cells were transfected with different combinations of plasmids carrying human Notch1, human GSK-3β and mouse VDAC1, along with Mitotracker. VDAC1-transfected cells

displayed very low intensity signal with only few cells that could be used for assessments of subcellular localization. While this is consistent with the WB experimetns, analysis was further complicated by the negative control sample loss in the process of sample preparation. In the selected cells VDAC1 localization clearly overlapped mitochondria, as would be expected from VDACs other than the mouse pl-VDAC1 variant.

Fluorescence of GSK-3β and Notch1 was much easier to differentiate from background, albeit less mitochondria-associated than VDAC1. GSK-3β appeared to be ubiquitously present within the cell with highest intensity in the cytoplasm and lower in the nucleus. Notch1 was present mostly in the cytoplasm compared to lower quantities in the membrane or nucleus. The lack of strong Notch1 signal in the membrane is not unusual, as this receptor

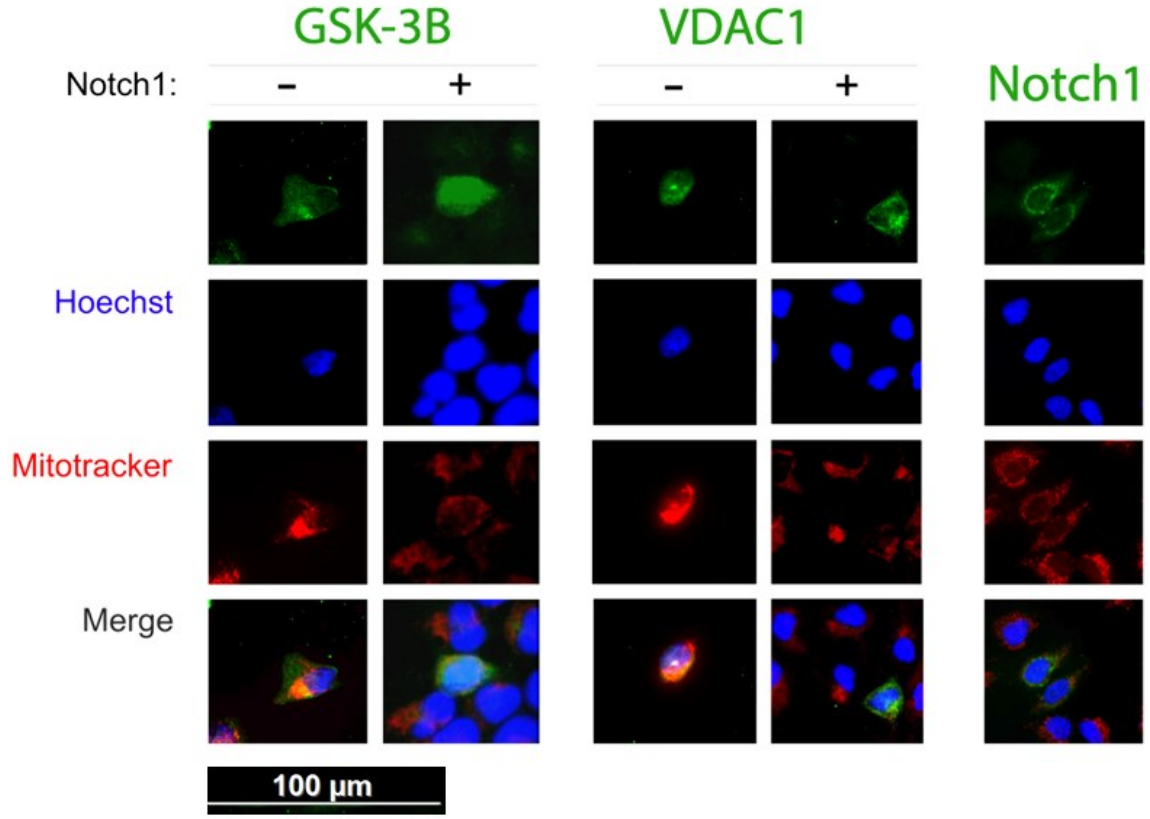

Fig. 13: Fluorescence imaging of transfected proteins and mitochondria. GSK-3 β localized throughout the whole cell also overlapping the mitochondria. VDAC1 localized mostly on mitochondria. Majority of Notch1 localized in the cytoplasm and indicated a partial overlap with mitochondria. Overexpressing Notch1 had no noticeable effect on localization of VDAC1 or GSK-3β. Images were adjusted independently for visibility; in unaltered images captured with identical exposure time the positive VDAC1 transfected cells would be less fluorescent than GSK-3 β or Notch1.

constantly undergoes dynamic vesicular trafficking. However, the spread of these two proteins indicates that some degree of overlap with each other and/or with mitochondria,

although quantification of the incidence would require confocal microscopy and probably higher quality samples.

This experiment served as a basic exploration of how the three proteins localize when transfected in HEK cells. It also shows that despite low expression, VDAC1 can be detected in mitochondria, something that would be more surprising knowing the nature of its splice "canonical" splice form.

4.7 Immunoprecipitation in HEK-293

Immunoprecipitation of pcDNA3.1hNOTCH1-HA and pcDNA3.1mVDAC1-FLAG transfected samples was attempted with the intention to confirm the presence of stable complexes in HEK cells but was unsuccessful due to low expression of VDAC1. NOTCH1-HA[2] successfully precipitated and the specificity was confirmed with WB detection of b-actin, which was present only in the untreated lysates (**Fig. 14**).

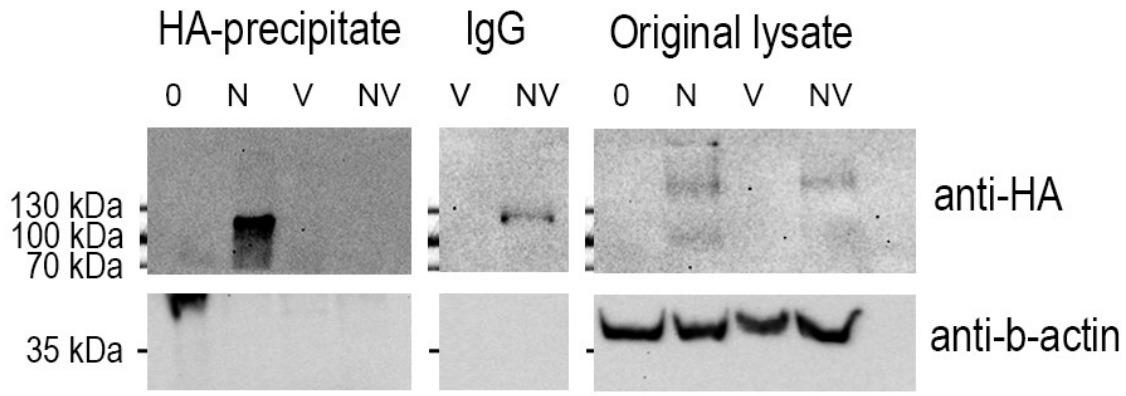

Fig. 14: Western blot detection of HA and actin after the immunoprecipitation experiment. Four samples were prepared – non-transfected (0), transfected with pcDNA3.1hNOTCH1-HA (N) or pcDNA3.1mVDAC1-FLAG (V) or co-transfected with both (NV). Part of each sample was precipitated through anti-HA mouse antibody; a visible band was detected only in N. Its absence in NV is unexpected as it was transfected with the same Notch1-coding plasmid and treated in the same conditions as N. Samples V and NV were also precipitated with non-specific mouse IgG and some non-specific signal was observed in NV. Notch1 was also detected in the expected untreated lysate

[2] Apparent MWs of Notch receptors on a western blot may seem unintuitive at first. Mature Notch is a heterodimer, broken down after lysis and denaturation. Used NOTCH1-HA tagged on the C-terminus and thus a band at around 120-130 kDa typically indicates the presence of full-length, mature Notch. Band at the "correct" 300 kDa indicates yet unprocessed Notch, before S1 cleavage. Released NICD itself weighs around 100-110 kDa and may appear as third band.

samples (N, NV). β-actin, present only in untreated lysates, indicates that it did not carry over to precipitated samples. VDAC1 bands were not visible in any sample and so the FLAG tag detection is not pictured. Images were adjusted for better visibility and serve no quantitative purpose.

Besides proteins in **Fig. 14**, some additional bands were observed. Most of these were determined to be antibody subunits carried over from precipitation and later bound by secondary antibodies. A band around 35 kDa was initially hypothesized to be VDAC but this idea was rejected because no such band appeared in untreated lysates.

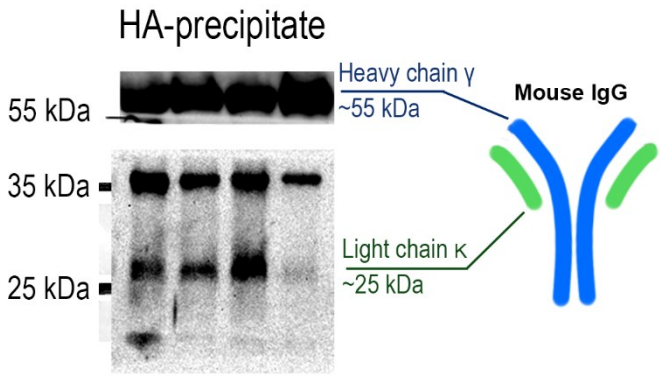

Fig. 15: Additional proteins detected in HA precipitates. Bands were present exclusively in precipitate lanes, consistently in blots incubated with different primary antibodies. Illustration of a (mouse) IgG on the right includes molecular mass of the two subunits.

Part 5: Discussion

5.1 Voltage-dependent anion channel 1

A plasmid for mammalian expression system containing mouse VDAC1 sequence has been prepared. Cloning of the splice variant known as pl-VDAC1 was unintended, but provided some interesting preliminary results, and may potentially serve as a useful tool for more detailed research. Attempts to express this variant in human cells yielded very low amounts of protein, while the fluorescence images suggest that the localization was mostly mitochondrial and no significant presence in the plasma membrane was detected. Characteristic double band is most likely the result of pl-VDAC1 being cleaved (or perhaps translation starting with the second methionine) and shows that the cleaved and non-cleaved proteins are present in comparable quantity. The third band was detected only in one experiment. The reason for this is unknown, a possibility is the presence of PTMs. For example, oxidized cysteine residues can affect electrophoretic mobility and can appear during the process of SDS-PAGE after treatment with reducing agents [131].

The western blot results in 3.2.4 are reminiscent of those in the original study characterizing mouse pl-VDAC1 [132]. On the other hand, immunolocalization images from the same publication differ from ours and show strong extramitochondrial signal. A likely explanation is the use of HEK-293, a human cell line. Processing of VDAC proteins is complicated and unexpected results have been reported. VDACs don't contain any mitochondrial targeting sequence and their correct localization is dependent on the function of various chaperons [133], [134]. For example, the unpredictable behavior of exogenous VDAC was reported in a Xenopus oocytes transfected with human VDAC1 [135]. The authors show how the expressed VDAC1 localized mostly in the plasma membrane, and these results were even partially dependent on the used protein tag. Cells also have multiple mechanisms that provide checkpoints and readjustments during protein localization, such as "ER-SURF" which redirects mislocated mitochondrial proteins from ER to the mitochondria [136].

Although human VDAC1 does not appear have any isoform equivalent to the pl-VDAC1 of mouse, plasmalemmal VDACs have been reported in human cells with a function that seems elusive and possibly related to disease [137]. Localization of VDAC was recently studied in the context of muscular dystrophy [138], while plasma membrane localized VDAC appear to have cytotoxic effects in neurons [139], [140]. Along with the evidence that pathogenesis

of myotonic dystrophy is largely mediated by impaired mRNA splicing [97], [141], studying how these mouse VDAC1 isoforms behave in human cells may be helpful for understanding neurodegenerative and muscular diseases. Designing and "troubleshooting" the (pl-)VDAC1 plasmid ended up being the majority of my thesis' experimental part but, with mt- variant in the process of cloning, more detailed look on VDAC1, its isoforms and mainly its protein-protein interactions can soon begin.

5.2 Glycogen synthase kinase-3 and Notch

The interaction between GSK-3 and Notch signaling is shown experimentally in multiple publications, most of them reviewed are in this thesis (**Table 1**). The conclusions of different studies are inconsistent and even methodically similar experiments on the same cell type have yielded opposite results. The reviewed studies are well designed and published in respected journals; there is not much reason to question the core results of any of them – GSK-3 can phosphorylate NICD (1 and 2), inhibiting GSK-3 can have consequences on Notch signaling that vary in their scale and mechanism depending on the biochemical context. We can, however, point out some possibly relevant factors that did not receive much discussion.

Articles rarely mention the characteristic structural features of GSK-3 even though they are well documented. One of them is the priming of its substrates. Most of the reported GSK-3 target residues on NICD are not within the common consensus sequence (S/T-X-X-X-Sp/Tp), which raises questions such as: is there a "primeable" residue that is further within the primary structure or is NICD an atypical, non-primed substrate? As the latter cannot be ruled out, GSK-3 may possibly act unexpectedly, for example when it comes to inhibition. Phosphorylation of N-terminal serine is mechanistically well characterized way inhibition of GSK-3 but measuring it (for example with phospho-specific antibodies) may not be an ideal assay of GSK-3 activity [142], [143]. This phosphoserine binds to the binding site, competing with primed substrates. However not every substrate of GSK-3 is primed, and these appear unaffected - notable example is AMP-activated protein kinase (AMPK) which was shown to be phosphorylated by pSer9-GSK-3β after Akt activation [28]. The most well-known and available GSK-3 inhibitor, lithium, has complex pharmacology and inhibits GSK-3 in several different ways, partially involving N-terminal serine phosphorylation [75] and thus, besides hypothetically affecting non-primed substrates differently, its physiological effects are not strictly related to GSK-3.

Unlike GSK-3, NICD structural insight is limited the RAM domain and Ankyrin repeats, while the unstructured c-terminal, part, containing multiple phosphorylation sites and the PEST domain, crucial for the NICD stability remains a challenge [126], [144], [145], [125]. Machine learning-based structure prediction is a rapidly growing field, and the accuracy of predictions is improving. However, as mentioned by the creators of Alphafold 3, its functionality is limited when it comes to proteins with disordered regions [118]. Demonstrated in section **4.1** , somewhat satisfiable results for NICD PPIs were achieved only when its C-terminal part (at least around 400 amino acids) was excluded.

5.3 A larger complex?

Using Alphafold 3 to predict relevant interactions produced more realistic-looking complexes, formed on top of the cytoplasmatic side of VDAC, than some previous attempts with Alphafold 2. Running Alphafold 3 with the sequences for VDAC1, GSK-3β, Grp75 (a component of VDAC1 complexes [146], in one study immunoprecipitated with N1ICD [128]) and N1ICD missing the TAD/PEST domains produced a model where the RAM domain of N1ICD interacts with Grp75, while GSK-3β approaches it from the C-terminal part, not too far from the reported residues in NLS (**Fig. 16**). Phosphorylating S2136 made it interact with GSK-3 β binding pocket, but the other residues were not correctly oriented towards the active site. In these models, Grp75 functioned as the central scaffold, which would be expected. However, to assess the accuracy, an experimentally determined structure of VDAC-Grp75 complex would be needed. Both VDAC1 and Grp75 have available structures but solving them together would be difficult, as they are usually part of the VDAC1-Grp75-IP3 complex – a contact site between mitochondria and ER.

In a mentioned study proteins in proximity of N2ICD have been analyzed at different times after its release [147]. The full data (Supplementary material) includes VDAC1, VDAC2, VDAC3 and other mitochondrial membrane proteins. However, their quantity peaked shortly after N2ICD release and, after 30 minutes, nuclear proteins started appearing and gradually replaced virtually all non-nuclear proteins identified in earlier samples. If NICD binds to proteins such as VDAC, the interaction is likely dynamic and short-lived. Nevertheless, the nature of cell's response to activated Notch is sensitive to alterations of NICD and even a small departure from NICD's canonical behavior could potentially be of relevance. Unfortunately, my immunoprecipitation experiment intended to test Notch1-VDAC1 interaction did not yield any results because of complications with plasmid. The sample with

VDAC1 and Notch1 lacked an observable band when precipitated, whether that was somehow related to the co-transfection would need to be tested by repeating the experiment. However it seems unlikely as there was almost no VDAC1 present in any samples. Bands detected around the size of VDAC1 were likely fragments of antibodies or even protein G (part of the beads used in immunoprecipitation) which would hypothetically bind antibodies non-specifically. The collected samples/blots could still have some value if specific VDAC antibodies were available – as that would allow for WB detection of endogenous VDAC.

Regardless, the suggested short-lived nature of NICD PPIs with components such as VDAC could also explain some discrepancy in the past research on GSK-3 and Notch. Even though timing is an important aspect of Notch signaling, it is difficult to study [148] and rarely given enough consideration.

Having prepared the needed toolset and methodology, we can start experimentally test some of the speculations above, ideally not only in HEK but also in DM patient muscle cells.

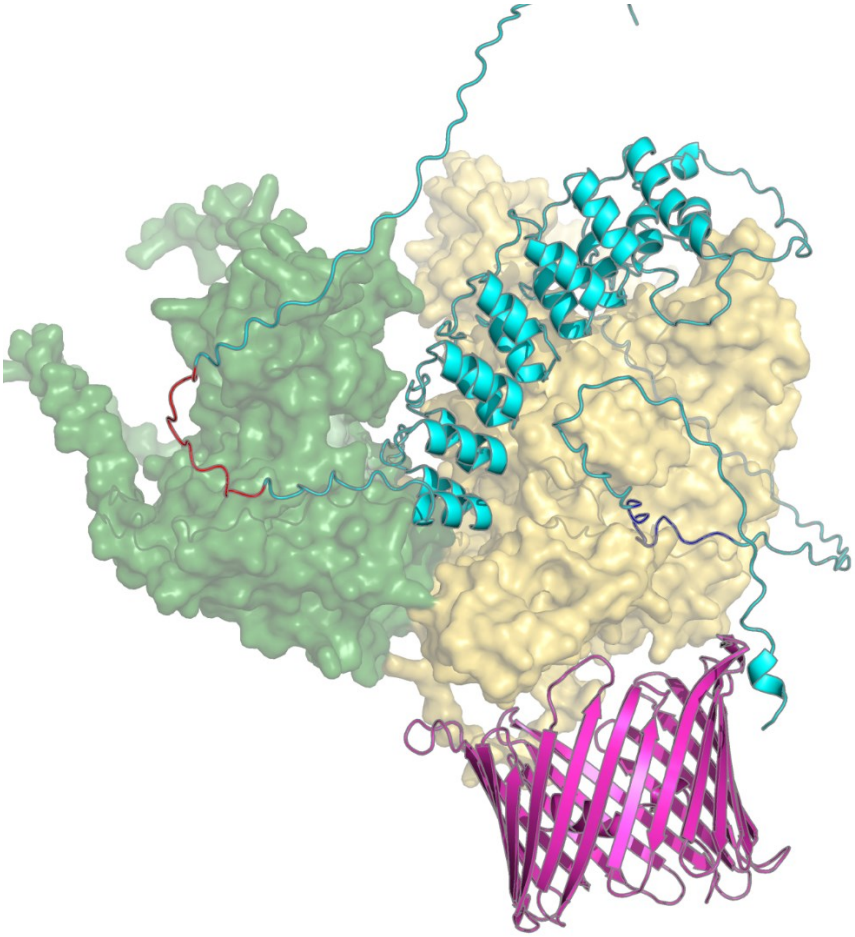

Fig. 16: Predicted complex of GSK-3 (green), N1ICD (cyan), VDAC1 (pink), Grp75 (yellow). The red part of N1ICD includes reported GSK-3 β phosphorylation sites, the blue part includes S1791 which was shown interacting with GSK-3 β in previous Alphafold predictions.

Part 6: Conclusions

Provided proteomic data were analyzed and VDAC1, reportedly a common interactor of Notch and GSK-3 potentially relevant in neurodegenerative and muscular diseases, was selected for future PPI-related experiments. The coding sequence of mouse VDAC1 was successfully amplified from a cDNA sample and inserted into a plasmid vector, along with FLAG tag on its C-terminus. Since the mouse and human VDAC1 are almost identical, this interaction between GSK-3β, N1ICD and VDAC1 was then studied in HEK cells (using transient transfection), however VDAC1 was expressed inadequately. The cause of this was later determined to be an additional N-terminal sequence specific to a minor splice variant of mouse VDAC1 which was unintentionally cloned instead of the standard variant highly conserved in various organisms.

References

[1] E. G. Krebs and E. H. Fischer, “The phosphorylase b to a converting enzyme of rabbit skeletal muscle,” *Biochim Biophys Acta*, vol. 20, no. 1, pp. 150–157, 1956, doi: 10.1016/0006-3002(56)90273-6.

[2] NobelPrize.org. Nobel Prize Outreach AB 2024, “The Nobel Prize in Physiology or Medicine 1992.” Accessed: May 10, 2024. [Online]. Available: https://www.nobelprize.org/prizes/medicine/1992/summary/

[3] G. Manning, D. B. Whyte, R. Martinez, T. Hunter, and S. Sudarsanam, “The protein kinase complement of the human genome,” *Science (1979)*, vol. 298, no. 5600, pp. 1912–1934, Dec. 2002, doi: 10.1126/SCIENCE.1075762/SUPPL_FILE/MANNINGSOM.PDF.

[4] J. D. R. Knight, B. Qian, D. Baker, and R. Kothary, “Conservation, Variability and the Modeling of Active Protein Kinases,” *PLoS One*, vol. 2, no. 10, p. 982, Oct. 2007, doi: 10.1371/JOURNAL.PONE.0000982.

[5] J. F. Markuns, J. F. P. Wojtaszewski, and L. J. Goodyear, “Insulin and Exercise Decrease Glycogen Synthase Kinase-3 Activity by Different Mechanisms in Rat Skeletal Muscle*,” *Journal of Biological Chemistry*, vol. 274, pp. 24896–24900, 1999, doi: 10.1074/jbc.274.35.24896.

[6] P. Cohen and S. Frame, “The renaissance of GSK3,” *Nature Reviews Molecular Cell Biology 2001 2:10*, vol. 2, no. 10, pp. 769–776, Oct. 2001, doi: 10.1038/35096075.

[7] N. EMBI, D. B. RYLATT, and P. COHEN, “Glycogen Synthase Kinase-3 from Rabbit Skeletal Muscle,” *Eur J Biochem*, vol. 107, no. 2, pp. 519–527, Jun. 1980, doi: 10.1111/J.1432-1033.1980.TB06059.X.

[8] T. R. Soderling, J. P. J. Icxenbottom, E. M. Reimann, F. L. Hunkeler, D. A. Walsh, and E. G. Krebs, “Inactivation of Glycogen Synthetase and Activation of Phosphorylase Kinase by Muscle Adenosine 3’, S-Monophosphate-dependent Protein Kinases*,” *Journal of Biological Chemistry*, vol. 245, no. 23, pp. 6317–6328, 1970, doi: 10.1016/S0021-9258(18)62612-2.

[9] H. G. Nimmo and P. Cohen, “Glycogen synthetase kinase 2 (GSK 2); the identification of a new protein kinase in skeletal muscle,” *FEBS Lett*, vol. 47, no. 1, pp. 162–166, Oct. 1974, doi: 10.1016/0014-5793(74)80450-3.

[10] P. COHEN, D. YELLOWLEES, A. AITKEN, A. DONELLA-DEANA, B. A. HEMMINGS, and P. J. PARKER, “Separation and Characterisation of Glycogen Synthase Kinase 3,Glycogen Synthase Kinase 4 and Glycogen Synthase Kinase 5 from Rabbit Skeletal Muscle,” *Eur J Biochem*, vol. 124, no. 1, pp. 21–35, May 1982, doi: 10.1111/J.1432-1033.1982.TB05902.X.

[11] E. Nikolakaki, P. J. Coffer, R. Hemelsoet, J. R. Woodgett, and L. H. K. Defize, “Glycogen synthase kinase 3 phosphorylates Jun family members in vitro and negatively regulates their transactivating potential in intact cells,” *Oncogene*, vol. 8, no. 4, 1993.

[12] D. P. Hanger, K. Hughes, J. R. Woodgett, J. P. Brion, and B. H. Anderton, “Glycogen synthase kinase-3 induces Alzheimer’s disease-like phosphorylation of tau: Generation of paired helical filament epitopes and neuronal localisation of the kinase,” *Neurosci Lett*, vol. 147, no. 1, pp. 58–62, Nov. 1992, doi: 10.1016/0304-3940(92)90774-2.

[13] E. Siegfried, T. Bin Chou, and N. Perrimon, “wingless signaling acts through zeste-white 3, the Drosophila homolog of glycogen synthase kinase-3, to regulate engrailed and establish cell fate,” *Cell*, vol. 71, no. 7, pp. 1167–1179, Dec. 1992, doi: 10.1016/S0092-8674(05)80065-0.

[14] M. Albert Basson, “Signaling in Cell Differentiation and Morphogenesis,” *Cold Spring Harb Perspect Biol*, vol. 4, no. 6, pp. 1–21, Jun. 2012, doi: 10.1101/CSHPERSPECT.A008151.

[15] E. Beurel, S. F. Grieco, and R. S. Jope, “Glycogen synthase kinase-3 (GSK3): regulation, actions, and diseases,” *Pharmacol Ther*, vol. 0, p. 114, 2015, doi: 10.1016/J.PHARMTHERA.2014.11.016.

[16] Z. Castaño, P. R. Gordon-Weeks, and R. M. Kypta, “The neuron-specific isoform of glycogen synthase kinase-3beta is required for axon growth,” *J Neurochem*, vol. 113, no. 1, pp. 117–130, Apr. 2010, doi: 10.1111/J.1471-4159.2010.06581.X.

[17] F. Mukai, K. Ishiguro, Y. Sano, and S. C. Fujita, “Alternative splicing isoform of tau protein kinase I/glycogen synthase kinase 3β,” *J Neurochem*, vol. 81, no. 5, pp. 1073–1083, Jun. 2002, doi: 10.1046/J.1471-4159.2002.00918.X.

[18] Y. Song *et al.*, “Regulatory network of GSK3-like kinases and their role in plant stress response,” *Front Plant Sci*, vol. 14, 2023, doi: 10.3389/FPLS.2023.1123436.

[19] R. Dajani *et al.*, “Crystal structure of glycogen synthase kinase 3β: Structural basis for phosphate-primed substrate specificity and autoinhibition,” *Cell*, vol. 105, no. 6, pp. 721–732, Jun. 2001, doi: 10.1016/S0092-8674(01)00374-9.

[20] B. Bax *et al.*, “The structure of phosphorylated GSK-3β complexed with a peptide, FRATtide, that inhibits β-catenin phosphorylation,” *Structure*, vol. 9, no. 12, pp. 1143–1152, 2001, doi: 10.1016/S0969-2126(01)00679-7.

[21] A. Bateman *et al.*, “UniProt: the Universal Protein Knowledgebase in 2023,” *Nucleic Acids Res*, vol. 51, no. D1, pp. D523–D531, Jan. 2023, doi: 10.1093/NAR/GKAC1052.

[22] B. W. Doble and J. R. Woodgett, “GSK-3: tricks of the trade for a multi-tasking kinase,” *J Cell Sci*, vol. 116, no. Pt 7, p. 1175, Apr. 2003, doi: 10.1242/JCS.00384.

[23] A. P. Kornev and S. S. Taylor, “Defining the Conserved Internal Architecture of a Protein Kinase,” *Biochim Biophys Acta*, vol. 1804, no. 3, p. 440, Mar. 2010, doi: 10.1016/J.BBAPAP.2009.10.017.

[24] B. Nolen, S. Taylor, and G. Ghosh, “Regulation of Protein Kinases: Controlling Activity through Activation Segment Conformation,” *Mol Cell*, vol. 15, no. 5, pp. 661–675, Sep. 2004, doi: 10.1016/J.MOLCEL.2004.08.024.

[25] E. Ter Haar, J. T. Coll, D. A. Austen, H. M. Hsiao, L. Swenson, and J. Jain, “Structure of GSK3beta reveals a primed phosphorylation mechanism,” *Nat Struct Biol*, vol. 8, no. 7, pp. 593–596, 2001, doi: 10.1038/89624.

[26] S. Frame, P. Cohen, and R. M. Biondi, “A common phosphate binding site explains the unique substrate specificity of GSK3 and its inactivation by phosphorylation,” *Mol Cell*, vol. 7, no. 6, pp. 1321–1327, Jun. 2001, doi: 10.1016/S1097-2765(01)00253-2.

[27] J. L. Stamos, M. L. H. Chu, M. D. Enos, N. Shah, and W. I. Weis, “Structural basis of GSK-3 inhibition by N-terminal phosphorylation and by the Wnt receptor LRP6,” *Elife*, vol. 2014, no. 3, Mar. 2014, doi: 10.7554/ELIFE.01998.

[28] T. Suzuki *et al.*, “Inhibition of AMPK catabolic action by GSK3,” *Mol Cell*, vol. 50, no. 3, p. 407, May 2013, doi: 10.1016/J.MOLCEL.2013.03.022.

[29] X. Fang, S. X. Yu, Y. Lu, R. C. Bast, J. R. Woodgett, and G. B. Mills, “Phosphorylation and inactivation of glycogen synthase kinase 3 by protein kinase A,” *Proc Natl Acad Sci U S A*, vol. 97, no. 22, pp. 11960–11965, Oct. 2000, doi: 10.1073/PNAS.220413597.

[30] “A Common Phosphate Binding Site Explains the Unique Substrate Specificity of GSK3 and Its Inactivation by Phosphorylation”.

[31] V. Stambolic and J. R. Woodgett, “Mitogen inactivation of glycogen synthase kinase-3 beta in intact cells via serine 9 phosphorylation,” *Biochem J*, vol. 303 (Pt 3), no. Pt 3, pp. 701–704, 1994, doi: 10.1042/BJ3030701.

[32] V. Stambolic and J. R. Woodgett, “Mitogen inactivation of glycogen synthase kinase-3 beta in intact cells via serine 9 phosphorylation,” *Biochem J*, vol. 303 (Pt 3), no. Pt 3, pp. 701–704, 1994, doi: 10.1042/BJ3030701.

[33] D. A. E. Cross, D. R. Alessi, P. Cohen, M. Andjelkovich, and B. A. Hemmings, “Inhibition of glycogen synthase kinase-3 by insulin mediated by protein kinase B,” *Nature*, vol. 378, no. 6559, pp. 785–789, Dec. 1995, doi: 10.1038/378785A0.

[34] A. R. Saltiel, “Insulin signaling in health and disease,” *J Clin Invest*, vol. 131, no. 1, Jan. 2021, doi: 10.1172/JCI142241.

[35] A. Cole, S. Frame, and P. Cohen, “Further evidence that the tyrosine phosphorylation of glycogen synthase kinase-3 (GSK3) in mammalian cells is an autophosphorylation event,” *Biochemical Journal*, vol. 377, no. 1, pp. 249–255, Jan. 2004, doi: 10.1042/BJ20031259.

[36] M. Aoki *et al.*, “Structural insight into nucleotide recognition in tau-protein kinase I/glycogen synthase kinase 3β,” *Acta Crystallographica Section D*, vol. 60, no. 3, pp. 439–446, Mar. 2004, doi: 10.1107/S090744490302938X.

[37] J. R. Miller, “The Wnts.,” *Genome Biol*, vol. 3, no. 1, pp. REVIEWS3001–REVIEWS3001, Dec. 2001, doi: 10.1186/GB-2001-3-1-REVIEWS3001.

[38] M. Kü hl, G. Editor, T. Purushothama Rao, and M. Kühl, “An Updated Overview on Wnt Signaling Pathways,” *Circ Res*, vol. 106, no. 12, pp. 1798–1806, Jun. 2010, doi: 10.1161/CIRCRESAHA.110.219840.

[39] R. Nusse *et al.*, “A new nomenclature for int-1 and related genes: the Wnt gene family,” *Cell*, vol. 64, no. 2, p. 231, Jan. 1991, doi: 10.1016/0092-8674(91)90633-A.

[40] “Pubmed Search: ‘wnt’. Acessed 11/5/2024.”

[41] R. Nusse and H. Clevers, “Wnt/β-Catenin Signaling, Disease, and Emerging Therapeutic Modalities,” *Cell*, vol. 169, no. 6, pp. 985–999, Jun. 2017, doi: 10.1016/J.CELL.2017.05.016.

[42] D. Strutt, D. Madder, V. Chaudhary, and P. J. Artymiuk, “Structure–Function Dissection of the Frizzled Receptor in Drosophila melanogaster Suggests Different Mechanisms of Action in Planar Polarity and Canonical Wnt Signaling,” *Genetics*, vol. 192, no. 4, p. 1295, Dec. 2012, doi: 10.1534/GENETICS.112.144592.

[43] S. Ikeda, S. Kishida, H. Yamamoto, H. Murai, S. Koyama, and A. Kikuchi, “Axin, a negative regulator of the Wnt signaling pathway, forms a complex with GSK-3beta and beta-catenin and promotes GSK-3beta-dependent phosphorylation of beta-catenin,” *EMBO J*, vol. 17, no. 5, pp. 1371–1384, Mar. 1998, doi: 10.1093/EMBOJ/17.5.1371.

[44] Y. Ahmed, A. Nouri, and E. Wieschaus, “Drosophila Apc1 and Apc2 regulate Wingless transduction throughout development,” *Development*, vol. 129, no. 7, pp. 1751–1762, 2002, doi: 10.1242/DEV.129.7.1751.

[45] C. Liu *et al.*, “Control of β-catenin phosphorylation/degradation by a dual-kinase mechanism,” *Cell*, vol. 108, no. 6, pp. 837–847, Mar. 2002, doi: 10.1016/S0092-8674(02)00685-2.

[46] W. Peterson-Nedry, N. Erdeniz, S. Kremer, J. Yu, S. Baig-Lewis, and M. Wehrli, “Unexpectedly robust assembly of the Axin destruction complex regulates Wnt/Wg signaling in Drosophila as revealed by analysis in vivo,” *Dev Biol*, vol. 320, no. 1, pp. 226–241, Aug. 2008, doi: 10.1016/J.YDBIO.2008.05.521.

[47] M. Ranes, M. Zaleska, S. Sakalas, R. Knight, and S. Guettler, “Reconstitution of the destruction complex defines roles of AXIN polymers and APC in β-catenin capture, phosphorylation, and ubiquitylation,” *Mol Cell*, vol. 81, no. 16, pp. 3246-3261.e11, Aug. 2021, doi: 10.1016/j.molcel.2021.07.013.

[48] V. W. Ding, R. H. Chen, and F. McCormick, “Differential regulation of glycogen synthase kinase 3β by insulin and Wnt signaling,” *Journal of Biological Chemistry*, vol. 275, no. 42, pp. 32475–32481, Oct. 2000, doi: 10.1074/jbc.M005342200.

[49] C. Metcalfe and M. Bienz, “Inhibition of GSK3 by Wnt signalling – two contrasting models,” *J Cell Sci*, vol. 124, no. 21, pp. 3537–3544, Nov. 2011, doi: 10.1242/JCS.091991.

[50] V. F. Taelman *et al.*, “Wnt Signaling Requires Sequestration of Glycogen Synthase Kinase 3 inside Multivesicular Endosomes,” *Cell*, vol. 143, no. 7, pp. 1136–1148, Dec. 2010, doi: 10.1016/J.CELL.2010.11.034.

[51] E. Y. Rim, L. K. Kinney, and R. Nusse, “β-catenin-mediated Wnt signal transduction proceeds through an endocytosis-independent mechanism,” *Mol Biol Cell*, vol. 31, no. 13, pp. 1425–1436, Jun. 2020, doi: 10.1091/MBC.E20-02-0114/ASSET/IMAGES/LARGE/MBC-31-1425-G005.JPEG.

[52] N. Tejeda-Muñoz and E. M. De Robertis, “Lysosomes are required for early dorsal signaling in the Xenopus embryo,” *Proc Natl Acad Sci U S A*, vol. 119, no. 17, p. e2201008119, Apr. 2022, doi: 10.1073/PNAS.2201008119/SUPPL_FILE/PNAS.2201008119.SAPP.PDF.

[53] J. S. Dexter, “The Analysis of a Case of Continuous Variation in Drosophila by a Study of Its Linkage Relations,” *https://doi.org/10.1086/279446*, vol. 48, no. 576, pp. 712–758, Dec. 1914, doi: 10.1086/279446.

[54] T. H. Morgan, “AMERICAN NATURALIST.” [Online]. Available: http://www.journals.uchicago.edu/t-an

[55] B. Zhou *et al.*, “Notch signaling pathway: architecture, disease, and therapeutics,” *Signal Transduction and Targeted Therapy 2022 7:1*, vol. 7, no. 1, pp. 1–33, Mar. 2022, doi: 10.1038/s41392-022-00934-y.

[56] R. Kopan and M. X. G. Ilagan, “The Canonical Notch Signaling Pathway: Unfolding the Activation Mechanism,” *Cell*, vol. 137, no. 2, pp. 216–233, Apr. 2009, doi: 10.1016/J.CELL.2009.03.045.

[57] D. Vlachakis, L. Papageorgiou, A. Papadaki, M. Georga, S. Kossida, and E. Eliopoulos, “An updated evolutionary study of the Notch family reveals a new ancient origin and novel invariable motifs as potential pharmacological targets,” *PeerJ*, vol. 8, Nov. 2020, doi: 10.7717/PEERJ.10334/SUPP-1.

[58] R. Sever and C. K. Glass, “Signaling by Nuclear Receptors,” *Cold Spring Harb Perspect Biol*, vol. 5, no. 3, Mar. 2013, doi: 10.1101/CSHPERSPECT.A016709.

[59] C. Zeng, S. Younger-Shepherd, L. Y. Jan, and Y. N. Jan, “Delta and Serrate are redundant Notch ligands required for asymmetric cell divisions within the Drosophila sensory organ lineage,” *Genes Dev*, vol. 12, no. 8, pp. 1086–1091, Apr. 1998, doi: 10.1101/GAD.12.8.1086.

[60] K. Sawamoto and H. Okano, “Cell-cell interactions during neural development: multiple types of lateral inhibitions involved in Drosophila eye development,”

Neurosci Res, vol. 26, no. 3, pp. 205–214, Nov. 1996, doi: 10.1016/S0168-0102(96)01110-8.

[61] M. Sjöqvist and E. R. Andersson, "Do as I say, Not(ch) as I do: Lateral control of cell fate," *Dev Biol*, vol. 447, no. 1, pp. 58–70, Mar. 2019, doi: 10.1016/J.YDBIO.2017.09.032.

[62] S. Sotillos, F. Roch, and S. Campuzano, "The metalloprotease-disintegrin Kuzbanian participates in Notch activation during growth and patterning of Drosophila imaginal discs," *Development*, vol. 124, no. 23, pp. 4769–4779, Dec. 1997, doi: 10.1242/DEV.124.23.4769.

[63] G. van Tetering, P. van Diest, I. Verlaan, E. van der Wall, R. Kopan, and M. Vooijs, "Metalloprotease ADAM10 is required for Notch1 site 2 cleavage," *J Biol Chem*, vol. 284, no. 45, pp. 31018–31027, Nov. 2009, doi: 10.1074/JBC.M109.006775.

[64] K. N. Lovendahl, S. C. Blacklow, and W. R. Gordon, "The molecular mechanism of notch activation," *Adv Exp Med Biol*, vol. 1066, pp. 47–58, 2018, doi: 10.1007/978-3-319-89512-3_3/COVER.

[65] K. Tamura *et al.*, "Physical interaction between a novel domain of the receptor Notch and the transcription factor RBP-Jκ/Su(H)," *Current Biology*, vol. 5, no. 12, pp. 1416–1423, Dec. 1995, doi: 10.1016/S0960-9822(95)00279-X.

[66] L. Wu, T. Sun, K. Kobayashi, P. Gao, and J. D. Griffin, "Identification of a Family of Mastermind-Like Transcriptional Coactivators for Mammalian Notch Receptors," *Mol Cell Biol*, vol. 22, no. 21, p. 7688, Nov. 2002, doi: 10.1128/MCB.22.21.7688-7700.2002.

[67] F. Logeat *et al.*, "The Notch1 receptor is cleaved constitutively by a furin-like convertase," *Proc Natl Acad Sci U S A*, vol. 95, no. 14, pp. 8108–8112, Jul. 1998, doi: 10.1073/PNAS.95.14.8108/ASSET/009C6B77-98CE-4BE0-BC51-0E6FB5E43A39/ASSETS/GRAPHIC/PQ1481625005.JPEG.

[68] A. Pandey, N. Niknejad, and H. Jafar-Nejad, "Multifaceted regulation of Notch signaling by glycosylation," *Glycobiology*, vol. 31, no. 1, p. 8, Jan. 2021, doi: 10.1093/GLYCOB/CWAA049.

[69] B. Sen Chen and C. C. Wu, "On the calculation of signal transduction ability of signaling transduction pathways in intracellular communication: systematic

approach," *Bioinformatics*, vol. 28, no. 12, pp. 1604–1611, Jun. 2012, doi: 10.1093/BIOINFORMATICS/BTS159.

[70] J. Mašek and E. R. Andersson, "The developmental biology of genetic Notch disorders," *Development*, vol. 144, no. 10, pp. 1743–1763, May 2017, doi: 10.1242/DEV.148007.

[71] P. Andersen, H. Uosaki, L. T. Shenje, and C. Kwon, "Non-Canonical Notch Signaling: Emerging Role and Mechanism," *Trends Cell Biol*, vol. 22, no. 5, p. 257, May 2012, doi: 10.1016/J.TCB.2012.02.003.

[72] H. K. Hing, X. Sun, and S. Artavanis-Tsakonas, "Modulation of wingless signaling by Notch in Drosophila," *Mech Dev*, vol. 47, pp. 261–268, 1994.

[73] L. Ruel, M. Bourouis, P. Heitzler, V. Pantesco, and P. Simpson, "Drosophila shaggy kinase and rat glycogen synthase kinase-3 have conserved activities and act downstream of Notch," *Nature 1993 362:6420*, vol. 362, no. 6420, pp. 557–560, 1993, doi: 10.1038/362557a0.

[74] D. R. Foltz, M. C. Santiago, B. E. Berechid, and J. S. Nye, "Glycogen synthase kinase-3β modulates notch signaling and stability," *Current Biology*, vol. 12, no. 12, pp. 1006–1011, Jun. 2002, doi: 10.1016/S0960-9822(02)00888-6.

[75] L. Freland and J. M. Beaulieu, "Inhibition of GSK3 by lithium, from single molecules to signaling networks," *Front Mol Neurosci*, vol. 5, no. JANUARY 2012, Jan. 2012, doi: 10.3389/FNMOL.2012.00014.

[76] L. Espinosa, J. Inglés-Esteve, C. Aguilera, and A. Bigas, "Phosphorylation by glycogen synthase kinase-3 beta down-regulates Notch activity, a link for Notch and Wnt pathways," *J Biol Chem*, vol. 278, no. 34, pp. 32227–32235, Aug. 2003, doi: 10.1074/JBC.M304001200.

[77] Y. H. Jin, H. Kim, M. Oh, H. Ki, and K. Kim, "Regulation of Notch1/NICD and Hes1 expressions by GSK-3α/β," *Mol Cells*, vol. 27, no. 1, pp. 15–19, Jan. 2009, doi: 10.1007/S10059-009-0001-7.

[78] W. Y. Kim *et al.*, "GSK-3 is a master regulator of neural progenitor homeostasis," *Nat Neurosci*, vol. 12, no. 11, pp. 1390–1397, Nov. 2009, doi: 10.1038/NN.2408.

[79] L. Zheng and S. D. Conner, "Glycogen synthase kinase 3β inhibition enhances Notch1 recycling," *Mol Biol Cell*, vol. 29, no. 4, pp. 389–395, Feb. 2018, doi: 10.1091/MBC.E17-07-0474.

[80] S. Guha *et al.*, “Glycogen synthase kinase 3 beta positively regulates Notch signaling in vascular smooth muscle cells: role in cell proliferation and survival,” *Basic Res Cardiol*, vol. 106, no. 5, pp. 773–785, Sep. 2011, doi: 10.1007/S00395-011-0189-5.

[81] F. De Falco *et al.*, “GSK3β is a critical, druggable component of the network regulating the active NOTCH1 protein and cell viability in CLL,” *Cell Death & Disease 2022 13:9*, vol. 13, no. 9, pp. 1–12, Sep. 2022, doi: 10.1038/s41419-022-05178-w.

[82] X. Han, J. hyun Ju, and I. Shin, “Glycogen synthase kinase 3-β phosphorylates novel S/T-P-S/T domains in Notch1 intracellular domain and induces its nuclear localization,” *Biochem Biophys Res Commun*, vol. 423, no. 2, pp. 282–288, Jun. 2012, doi: 10.1016/J.BBRC.2012.05.111.

[83] G. Lee, N. Cowan, and M. Kirschner, “The Primary Structure and Heterogeneity of Tau Protein from Mouse Brain,” *Science (1979)*, vol. 239, no. 4837, pp. 285–288, 1988, doi: 10.1126/SCIENCE.3122323.

[84] “Physiology and Pathology of Tau Protein Kinases in Relation to Alzheimer’s Disease.” Accessed: Apr. 28, 2024. [Online]. Available: https://www.jstage.jst.go.jp/article/biochemistry1922/121/2/121_2_179/_article

[85] H. Yu, M. Xiong, and Z. Zhang, “The role of glycogen synthase kinase 3 beta in neurodegenerative diseases,” *Front Mol Neurosci*, vol. 16, p. 1209703, Sep. 2023, doi: 10.3389/FNMOL.2023.1209703/BIBTEX.

[86] Q. Liao, Y. Zhang, J. He, and K. Huang, “Global Prevalence of Myotonic Dystrophy: An Updated Systematic Review and Meta-Analysis,” *Neuroepidemiology*, vol. 56, no. 3, pp. 163–173, Aug. 2022, doi: 10.1159/000524734.

[87] K. Jones *et al.*, “GSK3β mediates muscle pathology in myotonic dystrophy,” *J Clin Invest*, vol. 122, no. 12, p. 4461, Dec. 2012, doi: 10.1172/JCI64081.

[88] M. Lutz *et al.*, “Therapeutic Targeting of the GSK3β-CUGBP1 Pathway in Myotonic Dystrophy,” *International Journal of Molecular Sciences 2023, Vol. 24, Page 10650*, vol. 24, no. 13, p. 10650, Jun. 2023, doi: 10.3390/IJMS241310650.

[89] D. Vargas-Franco, R. Kalra, I. Draper, C. A. Pacak, A. Asakura, and P. B. Kang, “The Notch signaling pathway in skeletal muscle health and disease,” *Muscle Nerve*, vol. 66, no. 5, pp. 530–544, Nov. 2022, doi: 10.1002/MUS.27684.

[90] L. Den Hartog and A. Asakura, “Implications of notch signaling in duchenne muscular dystrophy,” *Front Physiol*, vol. 13, Sep. 2022, doi: 10.3389/FPHYS.2022.984373.

[91] S. Gioftsidi, F. Relaix, and P. Mourikis, “The Notch signaling network in muscle stem cells during development, homeostasis, and disease,” *Skeletal Muscle 2022 12:1*, vol. 12, no. 1, pp. 1–12, Apr. 2022, doi: 10.1186/S13395-022-00293-W.

[92] K. K. M. Roberts, “Myotonia.” Accessed: Apr. 30, 2024. [Online]. Available: https://www.ncbi.nlm.nih.gov/books/NBK559272/

[93] L. Machuca-Tzili, D. Brook, and D. Hilton-Jones, “Clinical and molecular aspects of the myotonic dystrophies: a review,” *Muscle Nerve*, vol. 32, no. 1, pp. 1–18, Jul. 2005, doi: 10.1002/MUS.20301.

[94] G. Meola and R. Cardani, “Myotonic dystrophies: An update on clinical aspects, genetic, pathology, and molecular pathomechanisms,” *Biochimica et Biophysica Acta (BBA) - Molecular Basis of Disease*, vol. 1852, no. 4, pp. 594–606, Apr. 2015, doi: 10.1016/J.BBADIS.2014.05.019.

[95] B. Udd and R. Krahe, “The myotonic dystrophies: molecular, clinical, and therapeutic challenges,” *Lancet Neurol*, vol. 11, no. 10, pp. 891–905, Oct. 2012, doi: 10.1016/S1474-4422(12)70204-1.

[96] S. Ait Benichou *et al.*, “Antisense oligonucleotides as a potential treatment for brain deficits observed in myotonic dystrophy type 1,” *Gene Ther*, vol. 29, no. 12, p. 698, Dec. 2022, doi: 10.1038/S41434-022-00316-7.

[97] E. M. Solovyeva *et al.*, “Integrative Proteogenomics for Differential Expression and Splicing Variation in a DM1 Mouse Model,” *Molecular & Cellular Proteomics*, vol. 23, no. 1, p. 100683, Jan. 2024, doi: 10.1016/J.MCPRO.2023.100683.

[98] A. Aoussim *et al.*, “Towards the Identification of Biomarkers for Muscle Function Improvement in Myotonic Dystrophy Type 1,” *J Neuromuscul Dis*, vol. 10, no. 6, p. 1041, Nov. 2023, doi: 10.3233/JND-221645.

[99] C. Siebel and U. Lendahl, “Notch signaling in development, tissue homeostasis, and disease,” *Physiol Rev*, vol. 97, no. 4, pp. 1235–1294, Oct. 2017, doi: 10.1152/PHYSREV.00005.2017/ASSET/IMAGES/LARGE/Z9J0041728220006.JPEG.

[100] M. A. Hill, “(24 Feb 24) Somitogenesis,” in *Embryology* , Retrieved from https://embryology.med.unsw.edu.au/embryology/index.php/Somitogenesis.

[101] K. F. Sonnen *et al.*, “Modulation of Phase Shift between Wnt and Notch Signaling Oscillations Controls Mesoderm Segmentation,” *Cell*, vol. 172, no. 5, p. 1079, Feb. 2018, doi: 10.1016/J.CELL.2018.01.026.

[102] J. von Maltzahn, N. C. Chang, C. F. Bentzinger, and M. A. Rudnicki, “Wnt Signaling in Myogenesis,” *Trends Cell Biol*, vol. 22, no. 11, p. 602, Nov. 2012, doi: 10.1016/J.TCB.2012.07.008.

[103] L. Nie *et al.*, “Directional induction of neural stem cells, a new therapy for neurodegenerative diseases and ischemic stroke,” *Cell Death Discovery 2023 9:1*, vol. 9, no. 1, pp. 1–22, Jul. 2023, doi: 10.1038/s41420-023-01532-9.

[104] R. Sueda and R. Kageyama, “Regulation of active and quiescent somatic stem cells by Notch signaling,” *Dev Growth Differ*, vol. 62, no. 1, pp. 59–66, Jan. 2020, doi: 10.1111/DGD.12626.

[105] K. Yang *et al.*, “The Key Roles of GSK-3β in Regulating Mitochondrial Activity,” *Cellular Physiology and Biochemistry*, vol. 44, no. 4, pp. 1445–1459, Dec. 2017, doi: 10.1159/000485580.

[106] L. Gomez *et al.*, “The SR/ER-mitochondria calcium crosstalk is regulated by GSK3β during reperfusion injury,” *Cell Death & Differentiation 2016 23:2*, vol. 23, no. 2, pp. 313–322, Jul. 2015, doi: 10.1038/cdd.2015.101.

[107] N. Haloi *et al.*, “Structural basis of complex formation between mitochondrial anion channel VDAC1 and Hexokinase-II,” *Communications Biology 2021 4:1*, vol. 4, no. 1, pp. 1–12, Jun. 2021, doi: 10.1038/s42003-021-02205-y.

[108] S. John, J. N. Weiss, and B. Ribalet, “Subcellular Localization of Hexokinases I and II Directs the Metabolic Fate of Glucose,” *PLoS One*, vol. 6, no. 3, p. e17674, 2011, doi: 10.1371/JOURNAL.PONE.0017674.

[109] H. Wang *et al.*, “Notch mediates the glycolytic switch via PI3K/Akt signaling to support embryonic development,” *Cell Mol Biol Lett*, vol. 28, no. 1, pp. 1–17, Dec. 2023, doi: 10.1186/S11658-023-00459-4/FIGURES/5.

[110] L. R. Perumalsamy, M. Nagala, and A. Sarin, “Notch-activated signaling cascade interacts with mitochondrial remodeling proteins to regulate cell survival,” *Proc Natl Acad Sci U S A*, vol. 107, no. 15, pp. 6882–6887, Apr. 2010, doi: 10.1073/PNAS.0910060107/SUPPL_FILE/SM03.AVI.

[111] A. Kasahara, S. Cipolat, Y. Chen, G. W. Dorn, and L. Scorrano, “Mitochondrial fusion directs cardiomyocyte differentiation via calcineurin and notch signaling,” *Science (1979)*, vol. 342, no. 6159, pp. 734–737, Nov. 2013, doi: 10.1126/SCIENCE.1241359/SUPPL_FILE/KASAHARA.SM.PDF.

[112] Y. Ito, M. Yamagata, T. Yamamoto, K. Hirasaka, T. Nikawa, and T. Sato, “The reciprocal regulation between mitochondrial-associated membranes and Notch signaling in skeletal muscle atrophy,” *Elife*, vol. 12, Dec. 2023, doi: 10.7554/ELIFE.89381.

[113] D. Szklarczyk *et al.*, “The STRING database in 2023: protein-protein association networks and functional enrichment analyses for any sequenced genome of interest,” *Nucleic Acids Res*, vol. 51, no. D1, pp. D638–D646, Jan. 2023, doi: 10.1093/NAR/GKAC1000.

[114] L. Kolberg, U. Raudvere, I. Kuzmin, P. Adler, J. Vilo, and H. Peterson, “g:Profiler—interoperable web service for functional enrichment analysis and gene identifier mapping (2023 update),” *Nucleic Acids Res*, vol. 51, no. W1, pp. W207–W212, Jul. 2023, doi: 10.1093/NAR/GKAD347.

[115] A. D. Shah, R. J. A. Goode, C. Huang, D. R. Powell, and R. B. Schittenhelm, “Lfq-Analyst: An easy-To-use interactive web platform to analyze and visualize label-free proteomics data preprocessed with maxquant,” *J Proteome Res*, pp. 204–211, 2019, doi: 10.1021/ACS.JPROTEOME.9B00496/SUPPL_FILE/PR9B00496_SI_001.PDF.

[116] R. Evans *et al.*, “Protein complex prediction with AlphaFold-Multimer,” *bioRxiv*, p. 2021.10.04.463034, Mar. 2022, doi: 10.1101/2021.10.04.463034.

[117] P. Bryant and F. Noé, “Rapid protein-protein interaction network creation from multiple sequence alignments with Deep Learning,” *bioRxiv*, p. 2023.04.15.536993, Apr. 2023, doi: 10.1101/2023.04.15.536993.

[118] J. Abramson *et al.*, “Accurate structure prediction of biomolecular interactions with AlphaFold 3,” *Nature 2024*, pp. 1–3, May 2024, doi: 10.1038/s41586-024-07487-w.

[119] Schrödinger LLC, “The PyMOL Molecular Graphics System, Version~1.8,” Nov. 2015.

[120] M. L. Hekkelman, I. de Vries, R. P. Joosten, and A. Perrakis, “AlphaFill: enriching AlphaFold models with ligands and cofactors,” *Nature Methods 2022 20:2*, vol. 20, no. 2, pp. 205–213, Nov. 2022, doi: 10.1038/s41592-022-01685-y.

[121] F. J. Martin *et al.*, “Ensembl 2023,” *Nucleic Acids Res*, vol. 51, no. D1, pp. D933–D941, Jan. 2023, doi: 10.1093/NAR/GKAC958.

[122] C. Camacho *et al.*, “BLAST+: architecture and applications,” *BMC Bioinformatics*, vol. 10, Dec. 2009, doi: 10.1186/1471-2105-10-421.

[123] P. Ranganathan *et al.*, “Hierarchical Phosphorylation within the Ankyrin Repeat Domain Defines a Phosphoregulatory Loop That Regulates Notch Transcriptional Activity,” *Journal of Biological Chemistry*, vol. 286, no. 33, pp. 28844–28857, Aug. 2011, doi: 10.1074/JBC.M111.243600.

[124] Y. Bian *et al.*, “An enzyme assisted RP-RPLC approach for in-depth analysis of human liver phosphoproteome,” *J Proteomics*, vol. 96, pp. 253–262, Jan. 2014, doi: 10.1016/J.JPROT.2013.11.014.

[125] D. R. Friedmann, J. J. Wilson, and R. A. Kovall, “RAM-induced Allostery Facilitates Assembly of a Notch Pathway Active Transcription Complex,” *J Biol Chem*, vol. 283, no. 21, p. 14781, May 2008, doi: 10.1074/JBC.M709501200.

[126] J. J. Wilson and R. A. Kovall, “Crystal structure of the CSL-Notch-Mastermind Ternary complex bound to DNA,” *Cell*, vol. 124, no. 5, pp. 985–996, Mar. 2006, doi: 10.1016/j.cell.2006.01.035.

[127] S. I. Hamstra, J. L. Braun, S. P. Chelko, and V. A. Fajardo, “GSK3-inhibition improves maximal SERCA activity in a murine model of Arrhythmogenic cardiomyopathy,” *Biochimica et Biophysica Acta (BBA) - Molecular Basis of Disease*, vol. 1868, no. 12, p. 166536, Dec. 2022, doi: 10.1016/J.BBADIS.2022.166536.

[128] N. Saini, S. Lakshminarayanan, P. Kundu, and A. Sarin, “Notch1 Modulation of Cellular Calcium Regulates Mitochondrial Metabolism and Anti-Apoptotic Activity in T-Regulatory Cells,” *Front Immunol*, vol. 13, p. 832159, Feb. 2022, doi: 10.3389/FIMMU.2022.832159/BIBTEX.

[129] S. Duvaud, C. Gabella, F. Lisacek, H. Stockinger, V. Ioannidis, and C. Durinx, “Expasy, the Swiss Bioinformatics Resource Portal, as designed by its users,” *Nucleic Acids Res*, vol. 49, no. W1, pp. W216–W227, Jul. 2021, doi: 10.1093/NAR/GKAB225.

[130] R. Z. Sabirov and P. G. Merzlyak, “Plasmalemmal VDAC controversies and maxi-anion channel puzzle,” *Biochimica et Biophysica Acta (BBA) - Biomembranes*, vol. 1818, no. 6, pp. 1570–1580, Jun. 2012, doi: 10.1016/J.BBAMEM.2011.09.024.

[131] C. Achilli, A. Ciana, and G. Minetti, “Oxidation of cysteine-rich proteins during gel electrophoresis,” *J Biol Methods*, vol. 5, no. 4, p. e104, Dec. 2018, doi: 10.14440/JBM.2018.275.

[132] R. Buettner, G. Papoutsoglou, E. Scemes, D. C. Spray, and R. Dermietzel, “Evidence for secretory pathway localization of a voltage-dependent anion channel isoform,” *Proc Natl Acad Sci U S A*, vol. 97, no. 7, pp. 3201–3206, Mar. 2000, doi: 10.1073/PNAS.97.7.3201/ASSET/ED394817-8509-417C-BCAF-63F8DBA9F84A/ASSETS/GRAPHIC/PQ0602422005.JPEG.

[133] A. Moitra and D. Rapaport, “The Biogenesis Process of VDAC – From Early Cytosolic Events to Its Final Membrane Integration,” *Front Physiol*, vol. 12, p. 732742, Aug. 2021, doi: 10.3389/FPHYS.2021.732742/BIBTEX.

[134] V. Kozjak-Pavlovic, K. Ross, N. Benlasfer, S. Kimmig, A. Karlas, and T. Rudel, “Conserved roles of Sam50 and metaxins in VDAC biogenesis,” *EMBO Rep*, vol. 8, no. 6, pp. 576–582, Jun. 2007, doi: 10.1038/SJ.EMBOR.7400982.

[135] C. Schwarzer *et al.*, “Human voltage-dependent anion-selective channel expressed in the plasmalemma of Xenopus laevis oocytes,” *Int J Biochem Cell Biol*, vol. 32, no. 10, pp. 1075–1084, Oct. 2000, doi: 10.1016/S1357-2725(00)00047-9.

[136] C. Koch, M. Schuldiner, and J. M. Herrmann, “ER-SURF: Riding the Endoplasmic Reticulum Surface to Mitochondria,” *Int J Mol Sci*, vol. 22, no. 17, Sep. 2021, doi: 10.3390/IJMS22179655.

[137] V. De Pinto, A. Messina, D. J. R. Lane, and A. Lawen, “Voltage-dependent anion-selective channel (VDAC) in the plasma membrane,” *FEBS Lett*, vol. 584, no. 9, pp. 1793–1799, May 2010, doi: 10.1016/J.FEBSLET.2010.02.049.

[138] R. Massa *et al.*, “Intracellular localization and isoform expression of the voltage-dependent anion channel (VDAC) in normal and dystrophic skeletal muscle,” *J Muscle Res Cell Motil*, vol. 21, no. 5, pp. 433–442, 2000, doi: 10.1023/A:1005688901635/METRICS.

[139] N. Akanda, R. Tofighi, J. Brask, C. Tamm, F. Elinder, and S. Ceccatelli, “Voltage-dependent anion channels (VDAC) in the plasma membrane play a critical role in apoptosis in differentiated hippocampal neurons but not in neural stem cells,” *Cell Cycle*, vol. 7, no. 20, pp. 3225–3234, Oct. 2008, doi: 10.4161/CC.7.20.6831.

[140] H. Koma, Y. Yamamoto, N. Okamura, and T. Yagami, “A plausible involvement of plasmalemmal voltage-dependent anion channel 1 in the neurotoxicity of 15-deoxy-Δ12,14-prostaglandin J2,” *Brain Behav*, vol. 10, no. 12, p. e01866, Dec. 2020, doi: 10.1002/BRB3.1866.

[141] M. K. Tanner, Z. Tang, and C. A. Thornton, “Targeted splice sequencing reveals RNA toxicity and therapeutic response in myotonic dystrophy,” *Nucleic Acids Res*, vol. 49, no. 4, pp. 2240–2254, Feb. 2021, doi: 10.1093/NAR/GKAB022.

[142] A. Krishnankutty *et al.*, “In vivo regulation of glycogen synthase kinase 3β activity in neurons and brains,” *Sci Rep*, vol. 7, no. 1, Dec. 2017, doi: 10.1038/S41598-017-09239-5.

[143] A. Ur Rahman Mohammed Abdul, B. De Silva, and R. K. Gary, “The GSK3 kinase inhibitor lithium produces unexpected hyperphosphorylation of β-catenin, a GSK3 substrate, in human glioblastoma cells,” *Biol Open*, vol. 7, no. 1, Jan. 2018, doi: 10.1242/BIO.030874.

[144] H. M. Berman *et al.*, “The Protein Data Bank,” *Nucleic Acids Res*, vol. 28, no. 1, pp. 235–242, Jan. 2000, doi: 10.1093/NAR/28.1.235.

[145] “www.rcsb.org; QUERY: Polymer Entity Description = ‘Neurogenic locus notch homolog protein 1’ OR Polymer Entity Description = ‘Neurogenic locus notch homolog protein 2’ OR Polymer Entity Description = ‘Neurogenic locus notch homolog protein 3’ OR Polymer Entity Description = ‘Neurogenic locus notch homolog protein 4.’”

[146] Q. Zhao *et al.*, “GRP75 Regulates Mitochondrial-Supercomplex Turnover to Modulate Insulin Sensitivity,” *Diabetes*, vol. 71, no. 2, pp. 233–248, Feb. 2022, doi: 10.2337/DB21-0173.

[147] A. P. Martin *et al.*, “A spatiotemporal Notch interaction map from plasma membrane to nucleus,” *Sci Signal*, vol. 16, no. 796, Aug. 2023, doi: 10.1126/SCISIGNAL.ADG6474/SUPPL_FILE/SCISIGNAL.ADG6474_MDAR_REPRODUCIBILITY_CHECKLIST.PDF.

[148] L. Tveriakhina *et al.*, “Temporal dynamics and stoichiometry in human Notch signaling from Notch synaptic complex formation to nuclear entry of the Notch intracellular domain,” *Dev Cell*, Apr. 2024, doi: 10.1016/J.DEVCEL.2024.03.021.

[149] "(glycogen synthase) NOT (kinase-3) - Search Results - PubMed." Accessed: Oct. 17, 2023. [Online]. Available: https://pubmed.ncbi.nlm.nih.gov/?term=%28glycogen+synthase%29+NOT+%28kinase-3%29

[150] P. V. Hornbeck, B. Zhang, B. Murray, J. M. Kornhauser, V. Latham, and E. Skrzypek, "PhosphoSitePlus, 2014: mutations, PTMs and recalibrations," *Nucleic Acids Res*, vol. 43, no. Database issue, pp. D512–D520, Jan. 2015, doi: 10.1093/NAR/GKU1267.

[151] P. Ranganathan *et al.*, "Hierarchical phosphorylation within the ankyrin repeat domain defines a phosphoregulatory loop that regulates Notch transcriptional activity," *J Biol Chem*, vol. 286, no. 33, pp. 28844–28857, Aug. 2011, doi: 10.1074/JBC.M111.243600.

[152] X. Han, J. hyun Ju, and I. Shin, "Glycogen synthase kinase 3-β phosphorylates novel S/T-P-S/T domains in Notch1 intracellular domain and induces its nuclear localization," *Biochem Biophys Res Commun*, vol. 423, no. 2, pp. 282–288, Jun. 2012, doi: 10.1016/J.BBRC.2012.05.111.

[153] C. J. Fryer, J. B. White, and K. A. Jones, "Mastermind Recruits CycC:CDK8 to Phosphorylate the Notch ICD and Coordinate Activation with Turnover," *Mol Cell*, vol. 16, no. 4, pp. 509–520, Nov. 2004, doi: 10.1016/J.MOLCEL.2004.10.014.

[154] H. Y. Choi *et al.*, "NOTCH localizes to mitochondria through the TBC1D15-FIS1 interaction and is stabilized via blockade of E3 ligase and CDK8 recruitment to reprogram tumor-initiating cells," *Experimental & Molecular Medicine 2024 56:2*, vol. 56, no. 2, pp. 461–477, Feb. 2024, doi: 10.1038/s12276-024-01174-6.

[155] R. Ujwal *et al.*, "The crystal structure of mouse VDAC1 at 2.3 Å resolution reveals mechanistic insights into metabolite gating," *Proc Natl Acad Sci U S A*, vol. 105, no. 46, pp. 17742–17747, Nov. 2008, doi: 10.1073/PNAS.0809634105/SUPPL_FILE/0809634105SI.PDF.

[156] M. Bayrhuber *et al.*, "Structure of the human voltage-dependent anion channel," *Proc Natl Acad Sci U S A*, vol. 105, no. 40, pp. 15370–15375, Oct. 2008, doi: 10.1073/PNAS.0808115105/SUPPL_FILE/0808115105SI.PDF.